



**Effect of microstructure and thread rolling on hydrogen embrittlement susceptibility  
in high strength steel fasteners**

**Fadi Saliby, ing.**

Department of Mining and Materials Engineering, McGill University, Montreal

A thesis submitted to McGill University in partial fulfillment of the requirements of the degree  
of Master in Engineering

July 2023

© Fadi Saliby, 2023

## **DEDICATION**

This work is dedicated to my family for their support and motivation.

Mom...it's finally done!

## **ABSTRACT**

High strength steel fasteners are susceptible to hydrogen embrittlement and can fail unexpectedly while in service. Hydrogen embrittlement is the result of a susceptible material exposed to hydrogen while subjected to tensile stresses. Preventing hydrogen embrittlement failures is critical in high and ultrahigh strength fasteners. Advancements in ultrahigh strength fastener technology targeting strength levels above 1400 MPa have led to development of bainitic microstructure for externally threaded fasteners. Lower bainite exhibits higher ductility and toughness than tempered martensite at equal strength. Susceptibility of a material to hydrogen embrittlement is directly related to the material condition, described by its strength, chemical composition, and microstructure. This research aims to compare the effect on susceptibility to hydrogen embrittlement of microstructures comprising tempered martensite and lower bainite. The effect of rolling threads before and after heat treatment on hydrogen embrittlement susceptibility is also examined. The experimental method used for this investigation is incremental step load (ISL) testing, in 4-point bending, with and without addition of hydrogen by cathodic charging. The methodology is designed to determine the hydrogen embrittlement threshold stress. Although at strength levels above 1200 MPa, both microstructures were very susceptible to hydrogen embrittlement, bainite exhibited marginally lower susceptibility than martensite. On the other hand, when the threads were rolled after heat treatment, resulting in significantly higher dislocation density by plastic deformation, results indicated significantly lower susceptibility, independent of the microstructure and hardness. This finding points to utilizing dislocations introduced by cold rolled threads as the most promising approach for minimizing hydrogen embrittlement susceptibility in ultrahigh strength steel fasteners.

## RÉSUMÉ

Les pièces de fixation en acier à haute résistance sont susceptibles à la fragilisation par l'hydrogène (FPH) et peuvent briser en opération de façon inattendue. Le mécanisme de la fragilisation par l'hydrogène est le résultat combiné de l'utilisation d'un matériau susceptible à la FPH exposé à l'hydrogène lorsqu'il est soumis à une contrainte en traction. La susceptibilité à la fragilisation par l'hydrogène est directement liée à l'état du matériau, c'est-à-dire ses propriétés mécaniques, à sa composition chimique et à sa microstructure. Cette recherche vise à comparer les effets de deux microstructures différentes sur la susceptibilité des pièces de fixation en acier à la fragilisation par l'hydrogène, c'est-à-dire la martensite revenue et la bainite inférieure. Cette recherche se penchera également sur l'effet des filets écrouis avant et après le durcissement par traitement thermique. La principale méthode utilisée pour cette étude est l'application de force en flexion par paliers. Cette méthode d'essai consiste de chargement en flexion à quatre points, avec et sans ajout de l'hydrogène par voie cathodique, pour mesurer le seuil de la fragilisation par l'hydrogène. Cette étude démontre que lorsque les filets sont écrouis avant le traitement thermique, la bainite inférieure offre une résistance à la FPH légèrement supérieure à -1.0 V de chargement cathodique. Lorsque les filets sont écrouis après le traitement thermique, la résistance à la FPH est supérieure en comparaison avec les pièces qui sont écrouies avant le traitement thermique, peu importe la microstructure ou les propriétés mécaniques. Les résultats démontrent aussi que les deux microstructures, à des niveaux de résistance supérieurs à 1200 MPa, sont très susceptibles à la FPH. Par ailleurs, pour les deux microstructures, l'écrouissage des filets après le traitement thermique réduit la susceptibilité à la FPH.

## **ACKNOWLEDGEMENTS**

I would like to start by thanking my supervisor Dr. Salim Brahim. He has supported me at every step of this project as well as in my professional career. He has guided me unselfishly. I would also like to thank Prof. Steve Yue for his valuable insight and guidance in my thesis review and Dr. Sriraman Rajagopalan for his assistance and support in my experimental work.

I would like to thank the industrial collaborators ITW, MNP, USCAR and Exova as well as Mitacs for their financial contribution.

Finally, I am most grateful to my wife, kids, mom and brothers for their encouragement.

## TABLE OF CONTENTS

ABSTRACT.....	i
RÉSUMÉ .....	ii
ACKNOWLEDGEMENTS .....	iii
TABLE OF CONTENTS.....	iv
LIST OF FIGURES AND TABLES.....	vii
Chapter 1 : Introduction .....	9
Chapter 2 : Literature Review .....	10
2.1 Basics of hydrogen embrittlement .....	10
2.1.1 Hydrogen Embrittlement and Conditions for HE Failure .....	10
2.1.2 Types of hydrogen embrittlement .....	11
2.1.3 Embrittlement damage mechanisms .....	13
2.1.4 Transport and trapping .....	13
2.1.5 Baking heat treatment .....	14
2.2 Microstructures for high strength fasteners – martensite and bainite .....	15
2.2.1 Martensite vs. bainite .....	15
2.3 Quantifying susceptibility to hydrogen embrittlement .....	19
2.3.1 Threshold stress .....	19
2.3.2 Measuring threshold stress by mechanical testing.....	19
2.3.3 Notch fracture strength evaluation.....	21
2.3.4 Other testing methods .....	21
2.4 Thread forming .....	22
2.4.1 Strain hardening effect of thread forming.....	22
Chapter 3 Experimental Method .....	24
3.1 Experimental methodology .....	24
3.2 ISL samples.....	25
3.3 ISL Apparatus .....	26

Chapter 4 : Materials.....	28
4.1 Description of specimen for ISL testing .....	28
4.2 Chemical composition .....	29
4.3 Hardness.....	30
4.4 Thread hardness .....	30
4.5 Tensile strength.....	30
Chapter 5 : Publication Strategy .....	35
5.1 Article 1 summary.....	35
5.2 Article 2 summary.....	35
5.3 Complementary data .....	36
Chapter 6 : ARTICLE 1: Hydrogen Embrittlement Susceptibility of Bainite for High Strength Steel Fasteners .....	37
6.1 Abstract.....	37
6.2 Introduction.....	37
6.3 Experimental Methodology .....	38
6.3.1 Measuring threshold stress by mechanical testing.....	38
6.3.2 Hydrogen charging conditions .....	40
6.3.3 Quantifying HE susceptibility.....	41
6.4 Material Conditions .....	42
6.5 Results.....	44
6.6 Discussion.....	47
6.7 Conclusions.....	48
6.8 References.....	49
Chapter 7 : ARTICLE 2: Effect of Rolling after Heat Treatment on Hydrogen Embrittlement Susceptibility for High Strength Steel Fasteners .....	51
7.1 Abstract.....	51
7.2 Introduction.....	51
7.3 Experimental Method.....	52
7.4 Material conditions .....	55
7.5 Results.....	59
7.5.1 Effect of rolling threads on NFS%.....	59
7.5.2 Effect of thread rolling on surface hardness .....	62
7.5.3 Fracture surface evaluation .....	63
7.6 Discussion.....	66

7.7 Conclusion .....	67
7.8 References.....	68
Chapter 8 : Discussion .....	70
8.1 Effect of lower bainite microstructure .....	70
8.2 Effect of rolling threads after heat treatment .....	71
Chapter 9 : Conclusions .....	73
Chapter 10 : Future work .....	74
10.1 Effect of microstructure – bainite vs. martensite .....	74
10.2 Effect of plastic deformation and dislocation density.....	74
References.....	75
Appendix 1: Complementary results.....	78
A1.1 Microstructure .....	78
A1.2 Fractography .....	81
A1.2.1 Fracture surface – -1.0 V Hydrogen Charging Condition – Rolled before HT – 45 HRC.....	81
A1.2.2 Fracture surface – -1.0 V Hydrogen Charging Condition – Rolled after HT – 39 HRC.....	83
A1.2.3 Fracture surface – -1.0 V H Charging Condition – Rolled after HT – 45 HRC.....	85
A1.3 Incremental Step Loading (ISL).....	88

## LIST OF FIGURES AND TABLES

### List of figures

Figure 2.1: Mechanism of galvanic corrosion of a zinc plated steel substrate [2]. Hydrogen is generated and absorbed in the steel substrate. ....	12
Figure 2.2: Comparing impact energy of lower bainite and tempered martensite for AISI 4340 at the same tensile strength shows increased toughness for lower bainite [3]. ....	15
Figure 2.3: Schematic representation of upper and lower bainite [22]. ....	17
Figure 2.4: Isothermal transformation diagram for 1080 steel [3]. ....	18
Figure 2.5: Schematic of a 4 point bending apparatus utilized for incremental load testing [29]. ....	20
Figure 2.6 : Schematic of an ISL graph showing the incremental step loading until sample fracture. ....	20
Figure 2.7: Spheroidizing temperature range on the iron carbon phase diagram [20]. ....	23
Figure 3.1: Example of the 4-point bending apparatus during testing in aqueous solution. ....	27
Figure 3.2: ISL loading profile in <i>Air</i> and under hydrogen charging conditions, i.e., $-1.2 V$ , $-1.0 V$ , $-0.9 V$ , at loading rate of $2\%-2h$ . ....	27
Figure 4.1: Hex flange head screw sample. ....	28
Figure 4.2: Heat treatment of tempered martensite (left) and lower bainite (right). ....	29
Figure 4.3: Core and thread hardness of rolled before and after HT of tempered martensite and lower bainite. ....	32
Figure 4.4: Machined tensile sample – modified ASTM E8-13a Fig. 8 Specimen 4. ....	32
Figure 4.5: Tensile test curves show a trend towards greater ductility for bainitic samples – Thread rolling before heat treatment. ....	33
Figure 4.6: Tensile test curves show a trend towards greater ductility for bainitic samples - thread rolling after heat treatment (lower hardness). ....	33
Figure 4.7: Tensile test curves show a trend towards greater ductility for bainitic samples - thread rolling after heat treatment (high hardness). ....	34
Figure 6.1: Incremental load testing apparatus. ....	39
Figure 6.2: Example of an ISL testing curve. ....	39
Figure 6.3: Hydrogen charging schematic condition. ....	41
Figure 6.4: Drawing of the screw (a). Actual supplied sample (b). ....	42
Figure 6.5: Heat treatment cycles for tempered martensite (a) and lower bainite (b). ....	43
Figure 6.6: Tempered martensite (a) and lower bainite (b) microstructure (500X / Nital 2%). ....	43
Figure 6.7: Machined tensile sample – modified ASTM E8-13a (Standard Test Methods for Tension Testing of Metallic Materials) [5] Fig. 8 Specimen 4. ....	44
Figure 6.8: Load vs. displacement curves for tempered martensite and lower bainite. ....	45
Figure 6.9: Bainite and martensite threshold loads at different cathodic charging conditions. ....	46
Figure 6.10: Percent notch fracture strength (NFS%) versus cathodic potential. ....	47
Figure 7.1: Schematic of incremental load testing apparatus. ....	53
Figure 7.2: Heat treatment of tempered martensite (left) and lower bainite (right). ....	55
Figure 7.3: Tempered martensite (left) and lower bainite (right) microstructures (Nital 2 %). ....	56
Figure 7.4: XRD on both martensite (B3, B5, B7) and lower bainite (B4, B6, B8) microstructures. ....	57
Figure 7.5: NFS% drop with increasing cathodic potential for both martensite and bainite when RBHT. Bainite showed less of an NFS% drop at $-1.0 V$ . ....	60

Figure 7.6: Comparison of NFS% drop with increasing cathodic potential for bainite when rolling before and after heat treatment. RAHT showed a less of a NFS% drop. ....	60
Figure 7.7: Comparison of NFS% drop with increasing cathodic potential for martensite when rolling before and after heat treatment. RAHT showed a less of a NFS% drop. ....	61
Figure 7.8: Comparison of NFS% drop with increasing cathodic potential for both bainite and martensite when rolling after heat treatment. RAHT showed slight reduction in NFS%. ....	61
Figure 7.9: Subsurface hardness profile showing the effect of thread rolling after heat treatment – converted from HV0.1. ....	62
Figure 7.10: Subsurface hardness profile showing the effect of thread rolling before heat treatment – converted from HV0.1. ....	63
Figure 7.11: Fracture propagation from initiation until final rupture - Lower bainite – RBHT – FF. ....	64
Figure 7.12: Fracture propagation from initiation until final rupture - Lower bainite – RBHT – Air. ....	65
Figure 7.13: Fracture propagation from initiation until final rupture - tempered martensite – RAHT – - 1.2V. ....	66

#### List of tables

Table 2.1: Mechanical properties comparison of 1095 steel. Bainite is shown to have higher impact strength as compared to tempered martensite at comparable hardness [20] .....	16
Table 4.1: Material conditions, including microstructure and thread rolling. ....	29
Table 4.2: Chemical composition .....	30
Table 4.3: Mechanical properties. ....	31
Table 6.1: Chemical composition .....	44
Table 7.1: Chemical composition for each group of samples. ....	58
Table 7.2: Material conditions, including microstructure and thread rolling. ....	58
Table 7.3: Mechanical properties. ....	58

## **Chapter 1 : Introduction**

High strength steel components are susceptible to hydrogen embrittlement (HE) and can fail suddenly during service. Understanding and managing the risk of this failure mechanism is critical.

Hydrogen embrittlement is the result of a susceptible material exposed to hydrogen while subjected to tensile stresses. Hydrogen may be absorbed during manufacturing steps such as acid pickling and electroplating as well as during in service corrosion. Baking heat treatments are used to remove or trap hydrogen in the material to reduce HE susceptibility. However, this step can add significant costs for longer baking times (up to 24 hrs). Susceptibility to HE is directly related to the material condition, notably strength, which is a function of chemistry and microstructure. The majority of industrial fasteners are produced with a tempered martensite microstructure while others are produced with lower bainite. Lower bainite has higher ductility and toughness compared to tempered martensite with equal hardness.

Industrial fastener threads are produced predominantly by cold forming (i.e., thread rolling) or in some cases by machining (i.e., material removal). Most industrial fasteners undergo a heat treatment after the manufacturing of the threads. In the scenario where the threads are rolled, it is referred to as threads rolled before heat treatment (RBHT). This manufacturing sequence is the most cost-effective approach. However, in bolted joint applications where dynamic service loads can initiate fatigue, threads are typically rolled after heat treatment (RAHT). Critical engine fasteners in the automotive industry and all aerospace fasteners fall into this category. Rolling threads after heat treatment introduces compressive residual stresses in the threads and increases fatigue life.

The first objective of this study is to investigate the effects of microstructure on susceptibility of steel fasteners to HE. More precisely, the study compares two microstructures, traditional quenched and tempered martensite and lower bainite obtained by austempering.

The second objective is to investigate the effect of rolling threads before and after heat treatment on HE susceptibility. The study looks at the effect of compressive stresses in the threads.

## **Chapter 2 : Literature Review**

The demand for higher strength steel is increasing across many sectors. For example, smaller fasteners with higher strength are gaining wider use in the auto industry to help reduce weight in cars thus increasing fuel efficiency. High strength and ultrahigh strength fasteners are very susceptible to hydrogen embrittlement (HE). Indeed, more than ever, the risk of HE must be managed to prevent catastrophic failures.

This review begins with a discussion of the fundamentals of HE. More precisely, the conditions required to cause HE failure, the two groupings of HE which depends on the hydrogen source, hydrogen damage mechanisms as well as diffusion and trapping of hydrogen. This is followed with a discussion of test methods for quantifying HE. Next, the two microstructures, i.e., tempered martensite and lower bainite, are described with an emphasis on detailing the small differences that distinguish the two from an HE perspective. Finally, the manufacturing process of rolling threads on mechanical fasteners is examined, with an emphasis of the effects of plastic deformation on hydrogen transport and trapping and susceptibility to hydrogen embrittlement.

### **2.1 Basics of hydrogen embrittlement**

#### **2.1.1 Hydrogen Embrittlement and Conditions for HE Failure**

Hydrogen embrittlement is a process by which different metals, notably high strength steel, when exposed to hydrogen that is absorbed, lose strength and/or ductility. The consequence of this phenomenon is a material that is rendered brittle and prone to cracking. For example, high strength steel fasteners that are hydrogen embrittled fracture at stresses that are below their normal strength, often unexpectedly while the fastener is in service.

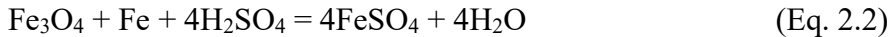
Hydrogen embrittlement of a component such as a steel fastener can only occur if the following three conditions are met: (i) the material must be susceptible to hydrogen damage, (ii) hydrogen must be present in the material, and (iii) the material must be under tensile stress. If any of these conditions is not met, or if one or a combination of the three conditions is sufficiently lowered, HE failure does not occur. Lastly, it is important to note that HE is a time dependent process. In other words, failure does not occur immediately on loading and occurs some time after the application of stress [1].

### 2.1.2 Types of hydrogen embrittlement

Hydrogen embrittlement is grouped into two categories based on the source of hydrogen: (1) internal hydrogen embrittlement (IHE) and (2) environmental hydrogen embrittlement (EHE)[2].

IHE occurs when hydrogen is introduced from manufacturing sources. For example, for the manufacturing of high strength fasteners, the following are possible sources of hydrogen [2] [3]:

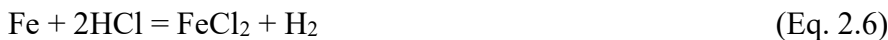
- Steelmaking: newly solidified metal is supersaturated with hydrogen originating from moisture [4]
- Acid pickling: Sulfuric acid ( $\text{H}_2\text{SO}_4$ ) and hydrochloric acid ( $\text{HCl}$ ) are used to remove any oxide scale prior to the spheroidizing process employed to soften the steel in preparation for cold forming. Sulfuric acid reacts with the iron oxides  $\text{FeO}$  and  $\text{Fe}_3\text{O}_4$  [5] according to Eq. 2.1 and 2.2:



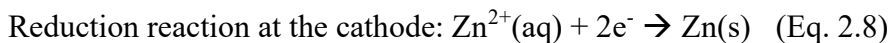
After the oxide reacts with the acid, the cathodic reaction at the surface of the base metal ( $\text{Fe}$ ) generates hydrogen gas ( $\text{H}_2$ ) according to Eq. 2.3 to 2.6:



Hydrochloric acid reacts similarly [5]



- Electroplating: Commercial zinc electroplating is accomplished predominantly in acid chloride or cyanide baths [5]. The basic reactions are according to Eq. 2.7 and 2.8:



The following electrolysis reaction occurs at the cathode if zinc ions are not promptly available for the electrons at the cathode: water is reduced to produce hydrogen ions and hydroxyl ions. Hydrogen ions can in turn be reduced to form atomic hydrogen which can diffuse into the coating and base metal, and molecular hydrogen which bubbles into the plating bath.



Molecules of  $\text{H}_2$  gas generated at the cathode are adsorbed onto the cathode surface. Dissociated hydrogen ions are then absorbed by the metal and diffuse in the matrix [6].

EHE is caused when hydrogen is introduced into the metal from an environmental source coupled with stress either residual or externally applied [7]. For example, during service, if a partially exposed steel substrate begins to corrode, reactions (9) and (10) are taking place (Figure 2.1).

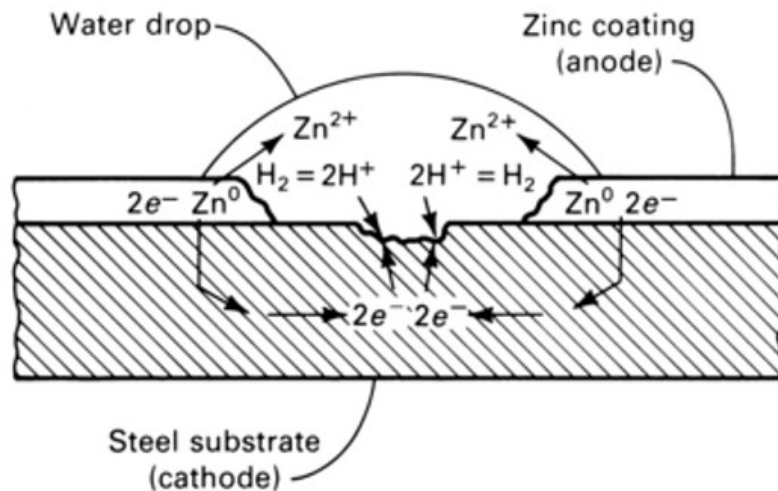


Figure 2.1: Mechanism of galvanic corrosion of a zinc plated steel substrate [2]. Hydrogen is generated and absorbed in the steel substrate.

### 2.1.3 Embrittlement damage mechanisms

Several theoretical models have been developed to describe the hydrogen damage mechanism in structural steel, notably *hydrogen gas pressure*, *atomic bond decohesion*, *enhanced plasticity* [2, 8].

The pressure theory was proposed by Zapffe and Sims [9]. It states that the accumulation of atomic hydrogen at microstructural defects promotes the formation of molecular hydrogen thereby causing micro cracking due to the hydrogen gas pressure. This mechanism occurs in lower strength structural steel (e.g., pipeline steel) and is not prevalent in high strength steel [2].

Hydrogen enhanced decohesion theory (HEDE) was first proposed by Troiano [10]. He proposed that accumulated hydrogen present ahead of the crack tip weakens bond between the metal atoms.

The hydrogen enhanced localized plasticity model (HELP) was first proposed by Beachem [10]. In this mechanism, hydrogen facilitates dislocation motion and therefore causes regions adjacent to the crack tip to plastically deform more readily.

### 2.1.4 Transport and trapping

Hydrogen embrittlement is a time dependent mechanism, resulting in delayed fracture. In other words, fracture occurs some amount of time after the application of stress. Time is necessary for hydrogen to move to the point of stress concentration (e.g., crack tip) and progressively cause damage.

At ambient temperature, stress induced hydrogen transport can occur by lattice diffusion in the matrix, driven by hydrostatic stress gradient, and facilitated by the small size of the hydrogen atom (atomic radius 53 pm). However, this mode of transport is relatively slower [11] than hydrogen transported by dislocations (i.e., pipe diffusion), which occurs by mere presence of hydrogen atoms in dislocations, without the need for a hydrostatic stress gradient as the driving force [12].

Hydrogen transport can be significantly affected by hydrogen “traps” in the microstructure. Different features in the microstructure of a metal become hydrogen traps, with varying trapping energies. These features include grain boundaries, precipitates, dislocations, voids, etc. Traps are classified as reversible (i.e., low binding energy) and irreversible (i.e., high binding energy).

Reversible traps can behave as sink or source of hydrogen. On the other hand, irreversible traps do not allow hydrogen to be released owing to their high binding energies [13]. Also, traps can be saturable or unsaturable [14]. Dislocations are considered reversible and saturable traps. Cracks and voids are considered reversible and unsaturable traps. The literature states diffusible and reversible hydrogen causes embrittlement whereas hydrogen in irreversible traps does not [15, 16].

### **2.1.5 Baking heat treatment**

High strength fastener manufacturing requires a heat treatment commonly called “baking” after electroplating. Baking is intended to eliminate the risk of IHE by either causing hydrogen to diffuse outward from the part or causing it to move to a trap site. The effectiveness of baking depends on temperature, duration and electroplated coating permeability to hydrogen. More precisely, higher temperatures, longer duration and greater permeability can separately or together increase the effectiveness of baking [17].

Although increasing temperature of baking is beneficial, heat of baking must not affect the mechanical properties of the fastener nor the performance of the coating. The duration of the baking operation must be sufficient to allow enough hydrogen to diffuse outward from the coated part or move to a high energy trap site. The industry standard for electroplating fasteners, ASTM F1941/F1941M [18], requires baking to be performed on fasteners with a minimum specified hardness above 39 HRC at temperatures ranging from 190 and 220°C (375 and 475°F). Minimum baking duration for parts with hardness up to 44 HRC is 14 hrs, and 24 hrs for hardness above 44 HRC. The coating permeability to hydrogen varies based on microstructural characteristics of the coating material, which in turn is determined by the coating process and electroplating parameters. For example, pure zinc electroplated coating has lower permeability to hydrogen than certain types of zinc nickel electroplating [17].

Industrial standards generally recommend that baking should be performed within hours after electroplating, as a matter of good practice, to avoid interstitial hydrogen from becoming trapped in reversible traps and more difficult to bake out [18].

## 2.2 Microstructures for high strength fasteners – martensite and bainite

### 2.2.1 Martensite vs. bainite

High strength steel fasteners are traditionally produced to have microstructure comprised of tempered martensite. A recent development for manufacturing ultrahigh strength fasteners (i.e., tensile strength 1400-1700 MPa) is the introduction of bainitic microstructure obtained by austempering [19]. Lower bainite has been shown to have higher ductility and toughness than tempered martensite at equal strength. Figure 2.2 and Table 2.1 show greater toughness of lower bainite as compared to tempered martensite (4340 steel and 1095 steel respectively).

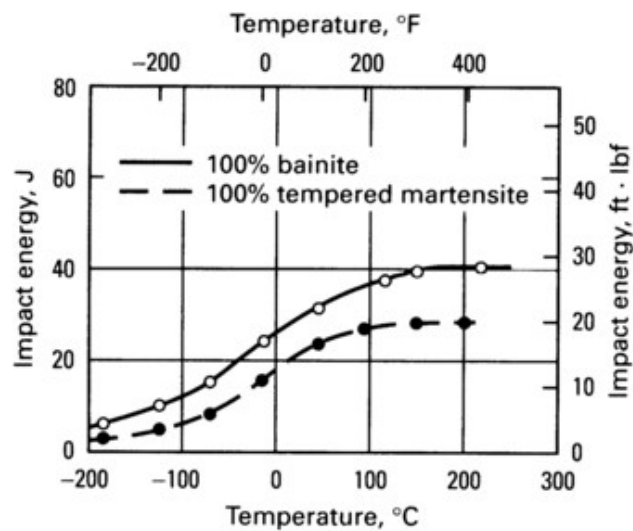


Figure 2.2: Comparing impact energy of lower bainite and tempered martensite for AISI 4340 at the same tensile strength shows increased toughness for lower bainite [3].

Table 2.1: Mechanical properties comparison of 1095 steel. Bainite is shown to have higher impact strength as compared to tempered martensite at comparable hardness [20]

Specimen no.	Heat treatment	Hardness, HRC	Impact strength		Elongation in 25 mm, or 1 in., %
			J	ft · lbf	
1	Water quenched and tempered	53.0	16	12	-
2	Water quenched and tempered	52.5	19	14	-
3	Bainite	52.0	61	45	11

Martensite is formed by rapidly cooling steel from the austenitizing temperature ranging from 815 to 870°C (1500 to 1600°F) to below the martensite finish temperature ( $M_f$ ) 100 to 200°C (212 to 392°F). It is a single-phase structure produced by a diffusionless transformation. The face centered cubic (FCC) austenite transforms to body centered tetragonal (BCT) martensite. The resulting structure is a supersaturated solid solution of carbon in iron. In the as quenched state, martensite is very hard, brittle with very high residual stress. A subsequent heat treatment, *tempering*, is performed at temperatures between 250 and 650°C (480 to 1200°F) which transforms the BCT structure into a partially recrystallized BCC (body centered cubic) structure that is strengthened by precipitated carbides, notably cementite. Consequently, the ductility and toughness of the resulting tempered martensite microstructure is substantially improved [21].

Bainite consists of ferrite and cementite phases and is formed by a combination of diffusionless and diffusion-based mechanisms. Bainite is formed by a process called austempering. Similar to martensite, rapid cooling is performed from austenitizing temperature ranging from 815 to 870°C (1500 to 1600°F) in a molten salt bath at temperatures above the start of martensite temperature ( $M_s$ ) and below that of pearlite formation. The temperature is maintained constant (isothermal transformation) until all the austenite transforms to bainite. Depending on the temperature chosen for the isothermal transformation, either lower or upper bainite is obtained. Lower bainite consists of needlelike ferrite plates that contain high densities of very fine carbide particles [3]. Upper bainite consists of coarse cementite particles between groups of ferrite laths. The objective for

desired properties is to obtain lower bainite [3]. Figure 2.3 shows a schematic of the transformation of both upper and lower bainite.

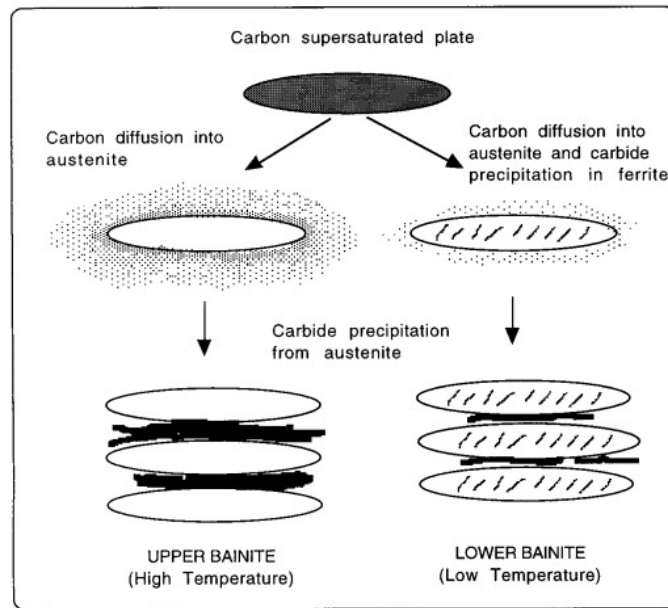


Figure 2.3: Schematic representation of upper and lower bainite [22].

Figure 2.4 shows an isothermal transformation diagram for 1080 steel. Fast cooling from the austenitic temperature (red line) to below  $M_s$  results in a martensitic microstructure. For austempering, after austenitizing, the steel is quenched in a salt bath to an intermediate temperature above  $M_s$  and held at that temperature until all the austenite transforms to lower bainite (purple line).

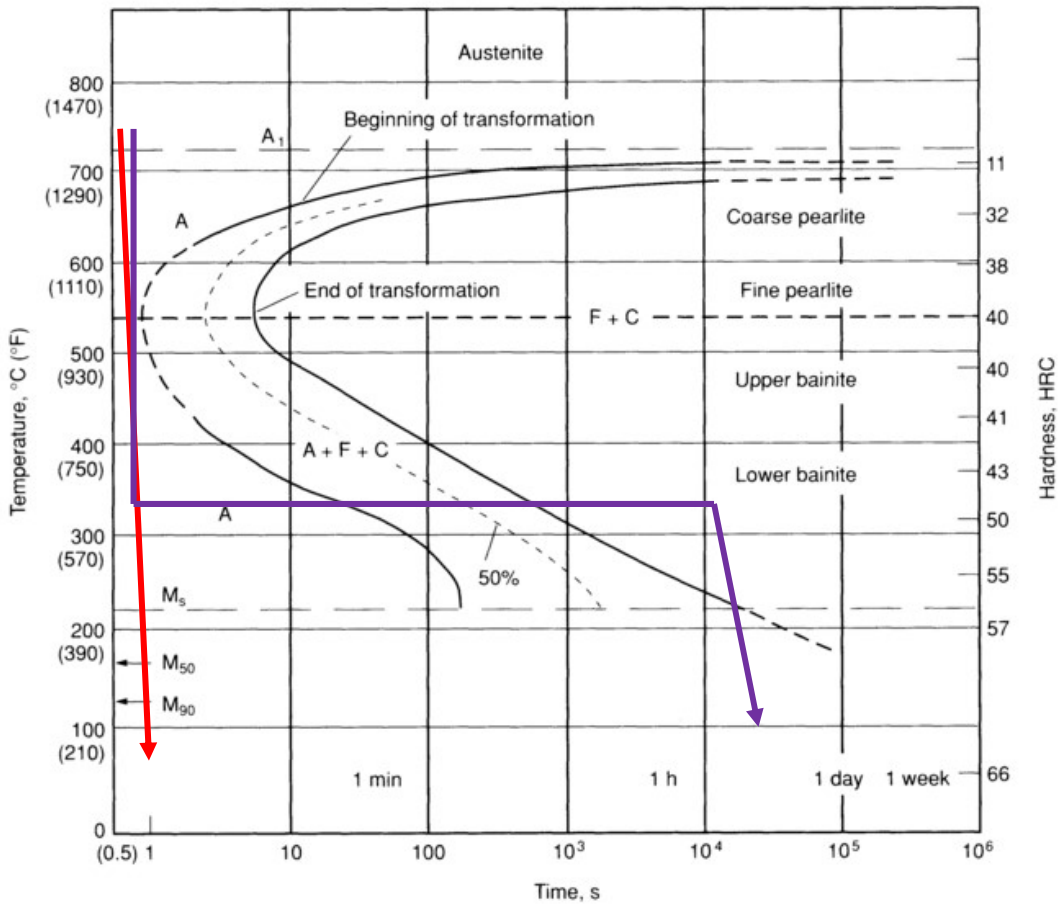


Figure 2.4: Isothermal transformation diagram for 1080 steel [3].

It was shown that for the same alloy, different microstructures have different resulting hydrogen transport and trapping behaviors [16]. Lower bainitic microstructures and mechanical properties (i.e., increased toughness and ductility) compared to tempered martensite might decrease its susceptibility to hydrogen embrittlement.

## **2.3 Quantifying susceptibility to hydrogen embrittlement**

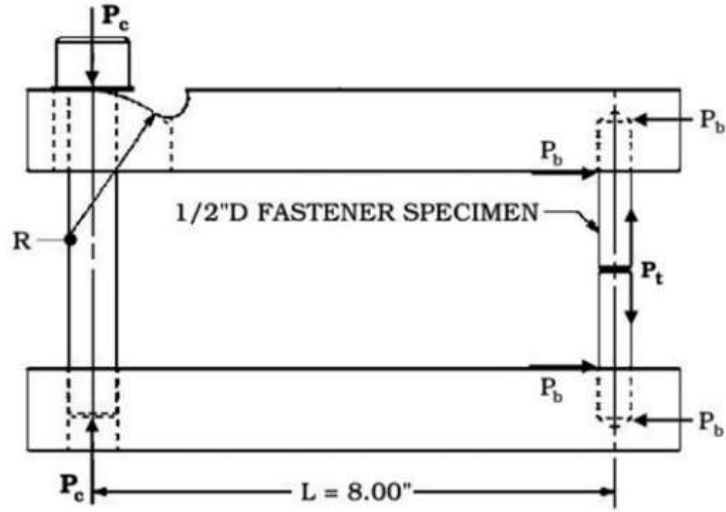
### **2.3.1 Threshold stress**

Hydrogen embrittlement susceptibility is quantified using fracture mechanics by measuring threshold stress intensity ( $K_{IHE}$ ). The threshold stress intensity results from the minimum applied stress needed to cause fracture for a given amount of hydrogen concentration. Stresses below the threshold stress do not cause fracture. Threshold stress is directly related to material strength and hydrogen concentration [2]. It has been shown that threshold stress decreases with increasing hydrogen concentration [23] and for a given concentration of hydrogen, threshold stress decreases with increasing material strength [2].

### **2.3.2 Measuring threshold stress by mechanical testing**

Since hydrogen embrittlement is a time dependent process, a test method whereby time and stresses are factors needs to be used. In the case of regular room temperature tensile tests based on ASTM E8 [24], testing times are not sufficient enough to detect the effects of hydrogen at ‘typical’ concentration levels. Thus the loading rate must be slow enough to allow hydrogen to diffuse, concentrate and cause damage [25].

Slow strain rate (SSR) and incremental strain loading (ISL) are two methods of quantifying threshold stress; the former are based on ISO 7539-7 [26] and ASTM G129 [27] while the latter is based on ASTM F1624 [28]. Both methods slowly increase load until failure of the sample. Testing can either be performed through tension or bending. Samples are notched or unnotched (i.e., smooth). Figure 2.5 shows a 4-point bending apparatus with incremental step loading control. Figure 2.6 shows an example of an incremental step loading graph.



NOTE 1—For Net Tensile Stress ( $\sigma_t$ ) in bending =  $\sigma_b$ ,  $P_t = 8M/d \geq 1.2P_{UTS-E8}$ , where  $M = LP_c$ .

Figure 2.5: Schematic of a 4 point bending apparatus utilized for incremental load testing [29].

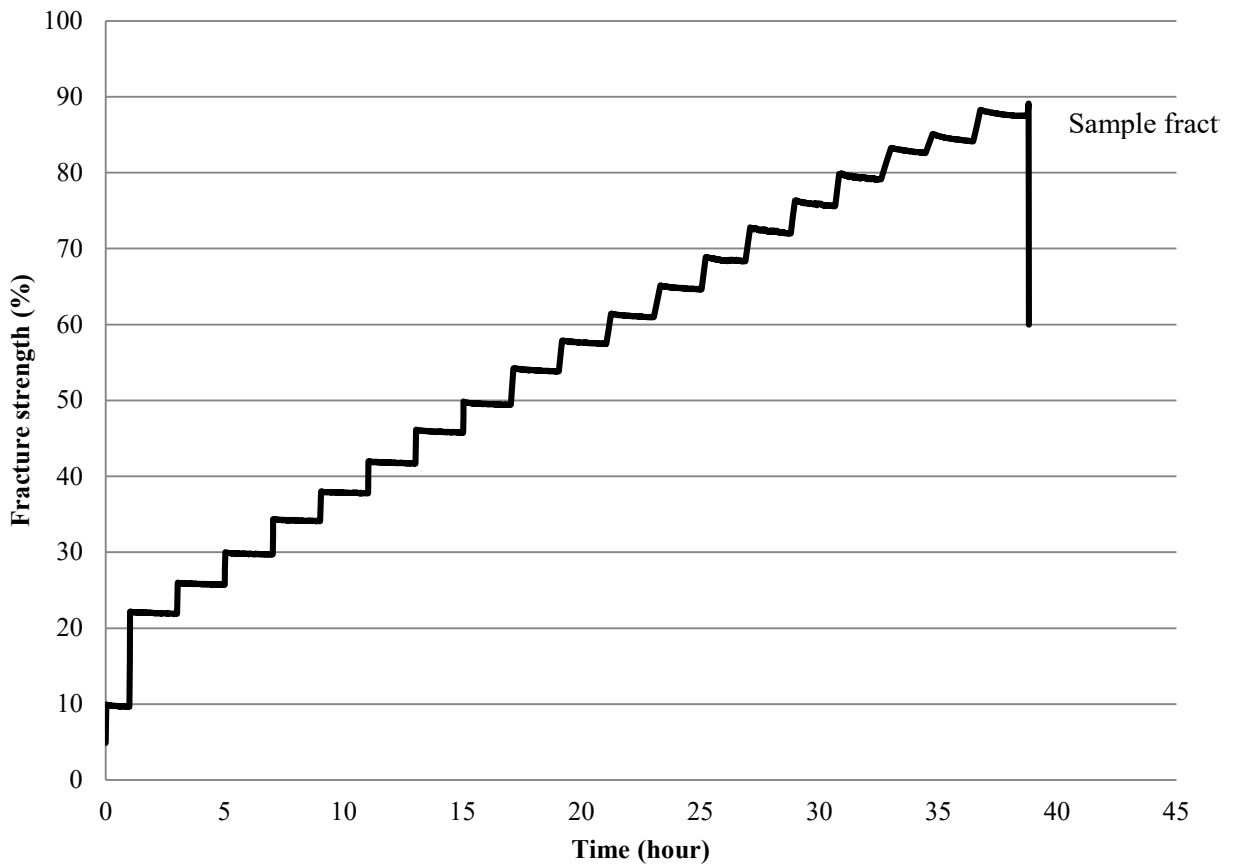


Figure 2.6 : Schematic of an ISL graph showing the incremental step loading until sample fracture.

Threshold stress measurement can be performed in air or in an aqueous environment under a hydrogen producing environment. Testing in air evaluates IHE whereas a hydrogen enriched environment evaluates EHE. One way of generating hydrogen is by imposing a cathodic potential in a 3.5% by weight sodium chloride solution. The electrochemical reaction causes hydrogen gas evolution. By varying the imposed potential, the concentration of hydrogen adsorbed by the sample varies. As the imposed potential decreases, the concentration of hydrogen adsorbed increases.

### 2.3.3 Notch fracture strength evaluation

Based on ASTM F1940 [30], HE susceptibility at a given hydrogen charging condition is quantified as follows:

$$NFS_{\%xxV} = \frac{ISL_{xxV}}{FF} \times 100 \quad (\text{Eq. 2.11})$$

Where

$NFS_{\%xxV}$  = Percent notch fracture strength at a specific hydrogen charging condition

$ISL_{xxV}$  = HE threshold fracture load

$FF$  = the baseline fast fracture load in air

$FF$  is performed in air while in bending at loading rate between 50 to 250 ksi/min (350 to 1700 MPa/min).  $ISL_{xxV}$  loading rates are based on ASTM F1624 [28]. Determining  $NFS_{\%xxV}$  reveals HE susceptibility (of a specific charging condition for EHE). F1940 states that any  $NFS$  below 75% reveals that the condition is potentially embrittling.

### 2.3.4 Other testing methods

#### 2.3.4.1 Sustained loading testing (SLT) - qualitative method suitable for production testing

In contrast to slow strain rate and incremental strain loading, sustained loading testing maintains a static load for the duration of the evaluation. Test duration can range from 24 hrs up to 200 hrs. It is a qualitative method where the result is pass or fail.

## **2.4 Thread forming**

### **2.4.1 Strain hardening effect of thread forming**

Strain hardening, obtained by plastic deformation, is produced by dislocation multiplication. Dislocation multiplication reduces dislocation mobility (or slip) and mechanical strength is then increased.

Prior to thread forming fasteners, a spheroidizing heat treatment is performed on the steel coil. Spheroidizing consists in heating between 675 to 875°C (1247 to 1607°F) (Figure 2.7) to allow the formation of a ductile microstructure, which enables easier cold forming. Once threads are cold formed, the local subsurface microstructure sees an increase in dislocation density. The subsequent heat treatment, used to produce martensite or bainite, involves heating the fasteners above the austenizing temperature where recovery and recrystallisation occurs, reverting the dislocation density back to the as-spheroidized condition.

In the case of critical bolted joints where dynamic service loads can initiate fatigue fractures, fastener threads are typically rolled after hardening. Examples of critical fasteners include engine and aerospace fasteners. Rolling threads after hardening introduces compressive residual stresses in the threads leading to increases in fatigue life [31, 32]. The accumulated dislocations generated at the subsurface of rolled threads after hardening could be very large hydrogen trap sites and therefore play a role in HE susceptibility. In addition, the introduction of compressive stress counteracts tensile forces, effectively reducing the applied tensile stress.

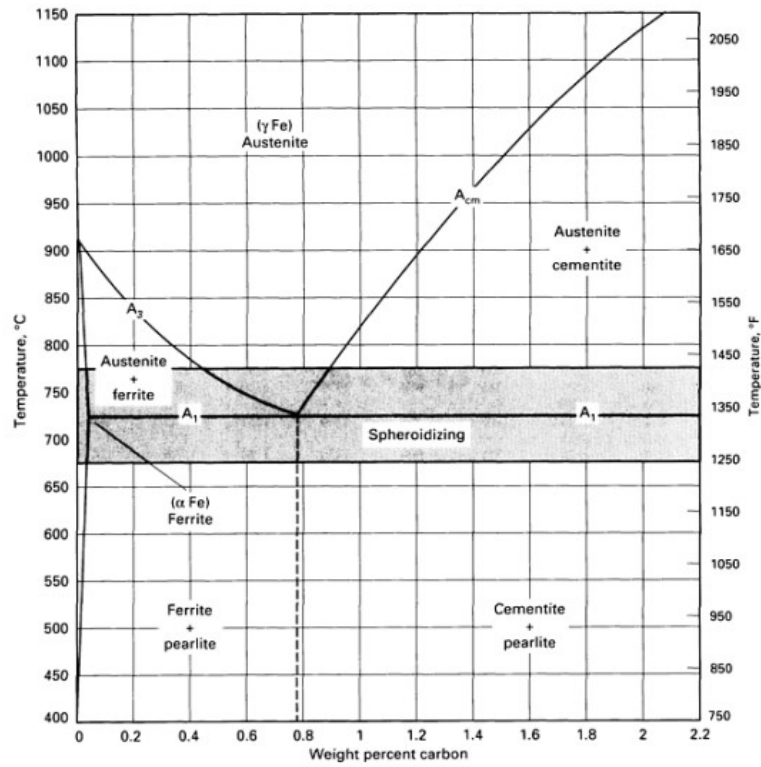


Figure 2.7: Spheroidizing temperature range on the iron carbon phase diagram [20].

## Chapter 3 Experimental Method

### 3.1 Experimental methodology

As indicated previously, the objective of this research is to evaluate HE susceptibility of high strength steel fasteners by investigating the effects of microstructure and rolled thread conditions. The principal mechanical testing method used for this investigation was incremental step load (ISL) 4-point bending with and without addition of hydrogen by cathodic charging to obtain HE threshold stresses. testing based on ASTM F1624 [28].

When the test is performed in air (i.e., without addition of hydrogen), only the effect of residual internal hydrogen present in the steel is measured. Under cathodic hydrogen charging conditions, the effect of varying amounts of additional environmental hydrogen is measured. This approach consists of imposing a cathodic potential in 3.5 % by weight sodium chloride solution. The sample is loaded in bending while immersed in this solution. The electrochemical reaction causes H<sub>2</sub> gas evolution and adsorption onto the surface of the sample (i.e., cathode). Atomic hydrogen is then absorbed by the material. Each sample is tested at a specific potential. By varying the imposed potential between -0.8 V and -1.2 V versus saturated calomel electrode (SCE), the concentration of hydrogen absorbed by the sample is varied. As the imposed potential is made more negative, the concentration of hydrogen generated at the cathode surface and absorbed by the sample is increased. The selection of imposed potentials between -0.8 V and -1.2 V was based on the equilibrium open circuit potential (OCP) of steel (approximately -0.65 V) and zinc (-1.20 V) in salt water [28].

The effect of hydrogen on the mechanical properties at a given hydrogen charging condition is quantified by the notch fracture strength (NFS), which is described by the following expression for cathodic charging potential of -1.2 V:

$$NFS_{\% -1.2 V} = \frac{ISL_{-1.2 V}}{FF} \times 100 \quad (\text{Eq. 3.1})$$

Where:

$NFS_{\% -1.2 V}$  is the percent notch fracture strength at a -1.2 V

$ISL_{-1.2 V}$  is the fracture load at a -1.2 V

FF is the baseline fast fracture load in air

When the test is performed at a sufficiently slow loading rate resulting in the lowest load,  $NFS_{\%xxV}$  is taken as the HE threshold. In this study, the loading protocol of steps comprising 2% load increments held for 2 hrs (i.e., 2%-2h) until fracture, was determined to reliably obtain the lowest fracture load.

The experimental steps are performed as follows.

- (1) Fast Fracture (FF): test using a rapid loading rate of 100 lbs /min - to establish the baseline strength. Given the speed of the test (i.e., 1-2 minutes), any hydrogen present does not have an effect.
- (2) ISL in air: test using a slow step loading rate in air (2%-2h) - to determine any effect of residual hydrogen that may have been present in the material.
- (3) ISL at -0.8 V, -1.0 V and -1.2 V: tests using a slow step loading rate (2%-2h) in a cathodic charging environment to measure the threshold strength under varying hydrogen charging conditions.

### 3.2 ISL samples

ISL specimens were prepared from the as received fasteners by sectioning off the fastener heads (Figure 3.1). This allowed the ISL specimens to be threaded into an ISL fixture. Only the threaded section at mid length was evaluated.

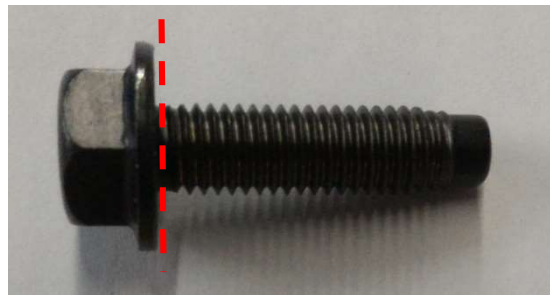


Figure 3.1: Location of cut to remove the head of the screw (i.e., dotted line). ISL testing was performed on thread section only.

### 3.3 ISL Apparatus

The test was conducted in a 4-point bending apparatus under displacement control (Figures 3.2 and 3.3). The apparatus was manufactured by Fracture Diagnostics Inc. Displacement and loads are computer controlled to  $\pm 0.13 \mu\text{m}$  and  $\pm 1.78 \text{ N}$  (0.4 lb) respectively. Load measurement is performed by a calibrated load cell with a maximum capacity of 2,224 N (500 lb). The test was stopped once a 5% drop in load was measured by the load cell, since this drop indicates initiation of cracking of the sample. Figure 3.4 shows an ISL loading curve of a specimen tested in air.

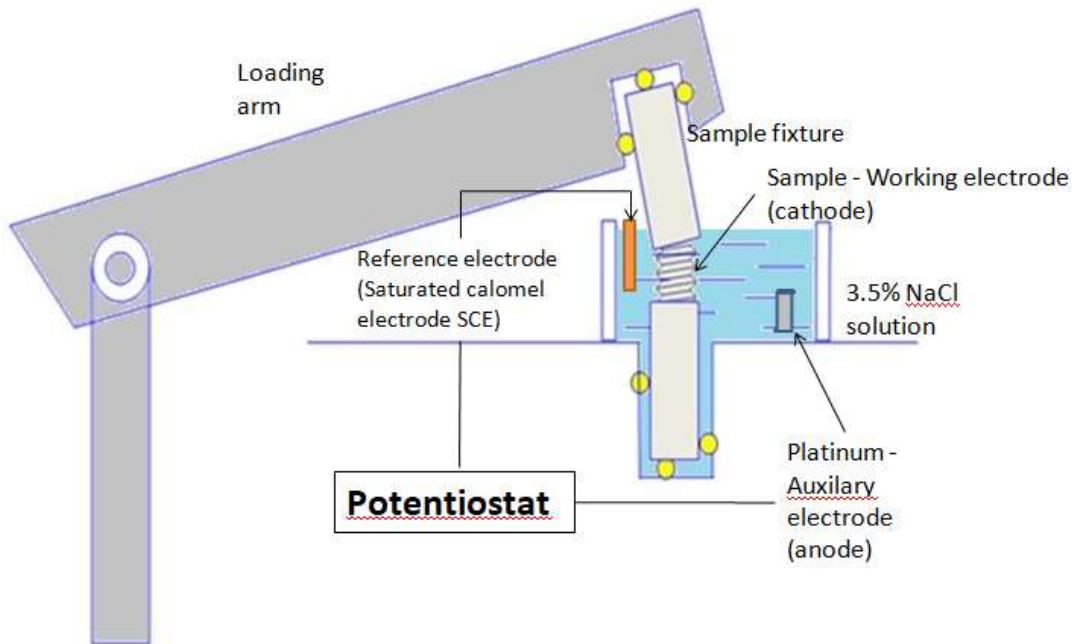


Figure 3.2: Schematic of a 4-point bending apparatus showing bending forces on a sample being cathodically charged while immersed in an aqueous solution under applied potential.

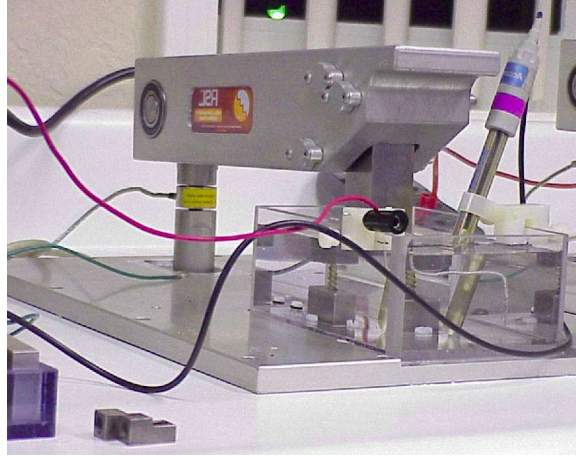


Figure 3.3: Example of the 4-point bending apparatus during testing in aqueous solution.

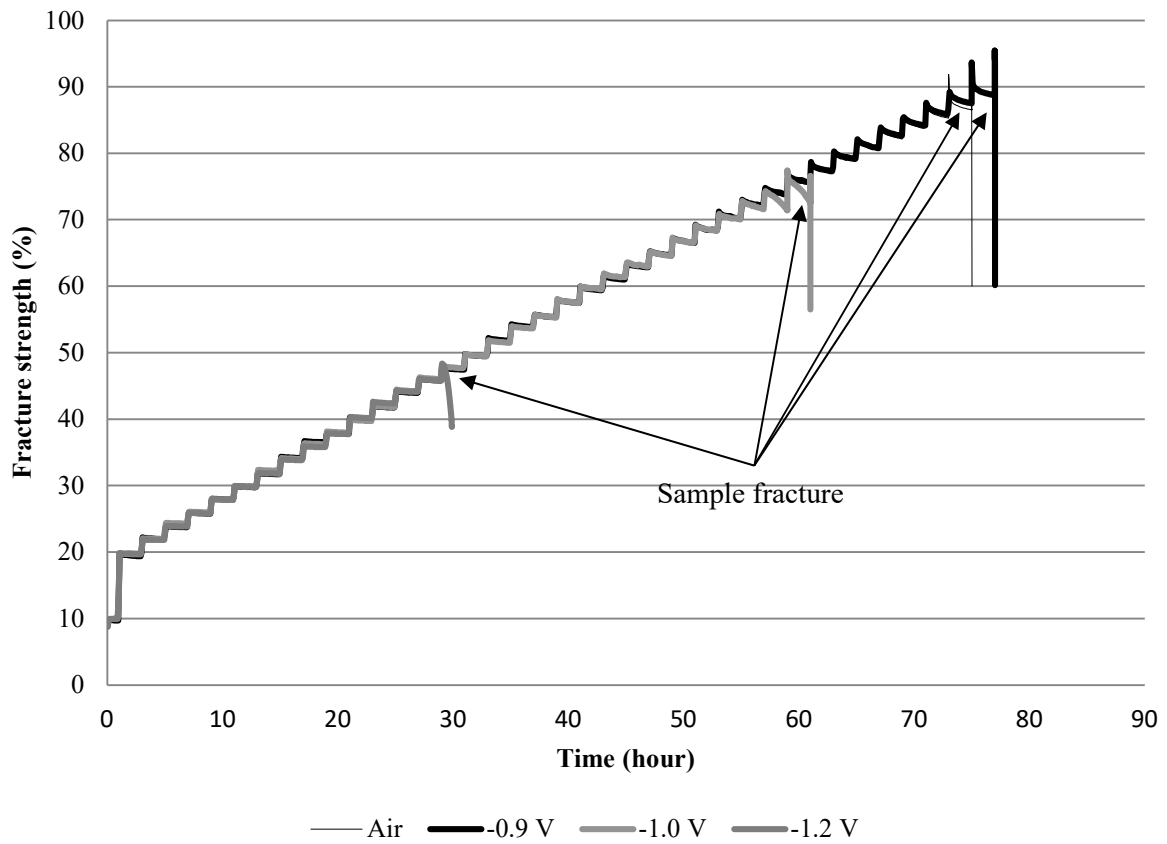


Figure 3.4: ISL loading profile in *Air* and under hydrogen charging conditions, i.e.,  $-1.2 V$ ,  $-1.0 V$ ,  $-0.9 V$ , at loading rate of  $2\%/2h$ .

## Chapter 4 : Materials

### 4.1 Description of specimen for ISL testing

Test specimens consisted of M8-1.25 X 30 mm high strength fasteners (Figure 4.1) fabricated by 2 different fastener manufacturers from AISI 8640 Ni-Cr-Mo steel alloy. The specimens were provided after heat treatment to form tempered martensite or lower bainite. The tempered martensite samples were austenitized at 865 °C, oil quenched and then tempered at 432°C for 45 minutes. The bainite samples were austenitized at 885 °C and quenched in a molten salt bath held at 364 °C for approximately 1 hour to achieve isothermal transformation (Figure 4.2). The specimens were also supplied with threads rolled before and after their respective final heat treatment condition. Table 4.1 shows the material condition including nominal hardness. The conditions to compare are the microstructure, hardness and rolling threads before and after final heat treatment.



Figure 4.1: Hex flange head screw sample.

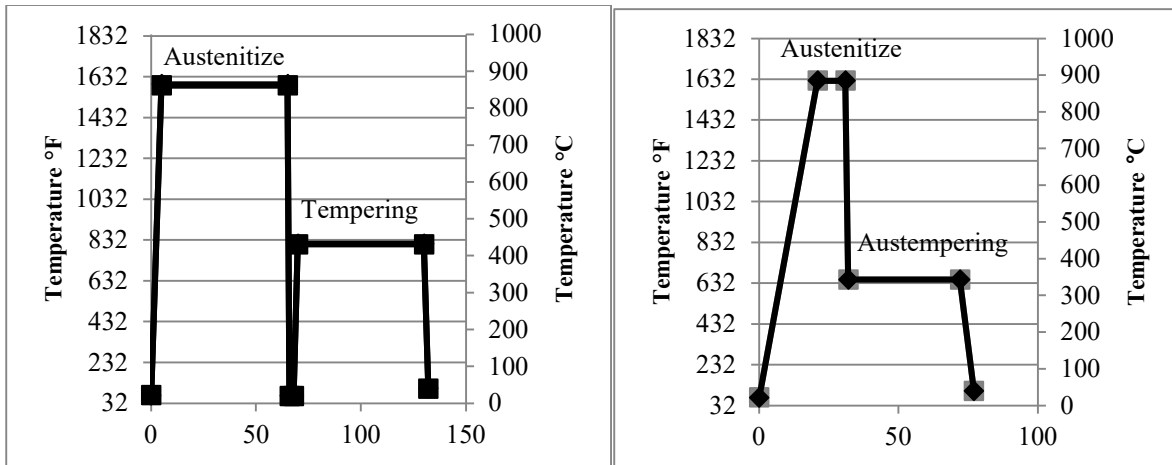


Figure 4.2: Heat treatment of tempered martensite (left) and lower bainite (right).

Table 4.1: Material conditions, including microstructure and thread rolling

Material ID	Microstructure	Nominal hardness (HRC)	Thread condition
1 B4	Lower Bainite	44	Rolled before heat treatment
2 B6		39	Rolled after heat treatment
3 B8		44	Rolled after heat treatment
4 B3	Tempered Martensite	44	Rolled before heat treatment
5 B7		39	Rolled after heat treatment
6 B9		44	Rolled after heat treatment

## 4.2 Chemical composition

The chemical composition of each material condition was determined by combustion analysis (carbon, sulfur and hydrogen) with an ELTRA CS-800 analyzer and inductively coupled plasma spectroscopy (ICP); (remaining elements) with a Thermo Scientific iCAP 6000 Series ICP Emission Spectrometer. Table 4.2 shows the chemical composition of each group of samples. The results confirm that the samples were AISI 8640 steel. In addition to the chemical elements of AISI 8640, residual hydrogen was also evaluated.

Table 4.2: Chemical composition

Material ID	Microstructure	% C	% Cr	% Mn	% Mo	% Ni	% P	% S	% Si	H (ppm)
1 B4	Lower Bainite	0.40	0.44	0.80	0.15	0.44	0.006	0.014	0.20	3.4
2 B6		0.44	0.50	0.95	0.18	0.48	0.011	0.002	0.22	1.8
3 B8		0.44	0.50	0.95	0.18	0.49	0.012	0.002	0.22	2.5
4 B3	Tempered Martensite	0.39	0.50	0.80	0.15	0.44	0.007	0.012	0.20	0.6
5 B7		0.44	0.50	0.94	0.18	0.50	0.011	0.002	0.22	0.8
4 B9		0.44	0.50	0.94	0.18	0.49	0.011	0.002	0.22	1.9
AISI 8640 Requirement		0.38-0.43	0.40-0.60	0.75-1.00	0.15-0.25	0.40-0.70	0.035 Max	0.040 Max	0.15-0.35	-

### 4.3 Hardness

The core hardness evaluation was performed per ASTM E18 [33] and ASTM F606 [34] on a United True-Blue tester. Measurements were conducted at the mid radius of a transverse section through the threads taken at an approximate distance of one diameter from the specimen end. The Rockwell hardness scale C (diamond indenter with a test force of 150 kgf) was utilized. Table 4.3 shows the mid radius hardness results of each group of samples. Figure 4.3 shows the core hardness comparison in all conditions.

### 4.4 Thread hardness

All measurements were performed in the thread root by micro hardness per ASTM E384 [35] and ASTM F606 [34] on a Buehler 1600-6400 MicroMet tester. The Vickers hardness scale was utilized with a test force of 100 gf. Table 4.3 shows the thread hardness results of each group of samples. Figure 4.3 shows the thread hardness in all conditions.

### 4.5 Tensile strength

Tensile strength was measured per ASTM E8 [24] on an Instron 600DX. Tensile specimens were machined from the fasteners (Figure 4.4). Dimensions were based on a modified version of Specimen 4 in ASTM E8 [24]. Table 4.3 shows the tensile, elongation and reduction of area of

each group of samples. Figures 4.5 to 4.7 show the load versus displacement graphs. In all conditions, the lower bainite samples showed higher displacement (i.e., ductility) over tempered martensite at comparable hardness.

Table 4.3: Mechanical properties

Material ID	Microstructure	Hardness (Mid radius HRC)	Surface Hardness (converted from HV0.1kg to HRC) at 51 $\mu\text{m}$	Tensile Strength (MPa)	Elongation (%)	Reduction of area (%)
1 B4	Lower Bainite	$46.6 \pm 0.3$	$46.9 \pm 1.0$	$1562 \pm 12$	$19.4 \pm 3.8$	$27.4 \pm 4.4$
2 B6		$39.3 \pm 0.4$	$48.9 \pm 0.6$	$1294 \pm 8$	$18.9 \pm 1.5$	$37.4 \pm 0.6$
3 B8		$43.6 \pm 0.2$	$52.1 \pm 1.9$	$1440 \pm 15$	$13.7 \pm 1.8$	$31.8 \pm 1.1$
4 B3	Tempered Martensite	$45.2 \pm 0.4$	$47.4 \pm 0.7$	$1521 \pm 6$	$12.0 \pm 1.7$	$21.2 \pm 0.3$
5 B7		$38.2 \pm 1.1$	$47.8 \pm 0.9$	$1272 \pm 7$	$19.0 \pm 0.1$	$33.1 \pm 0.1$
6 B9		$43.7 \pm 0.5$	$50.3 \pm 1.3$	$1456 \pm 10$	$17.0 \pm 2.8$	$27.8 \pm 3.2$

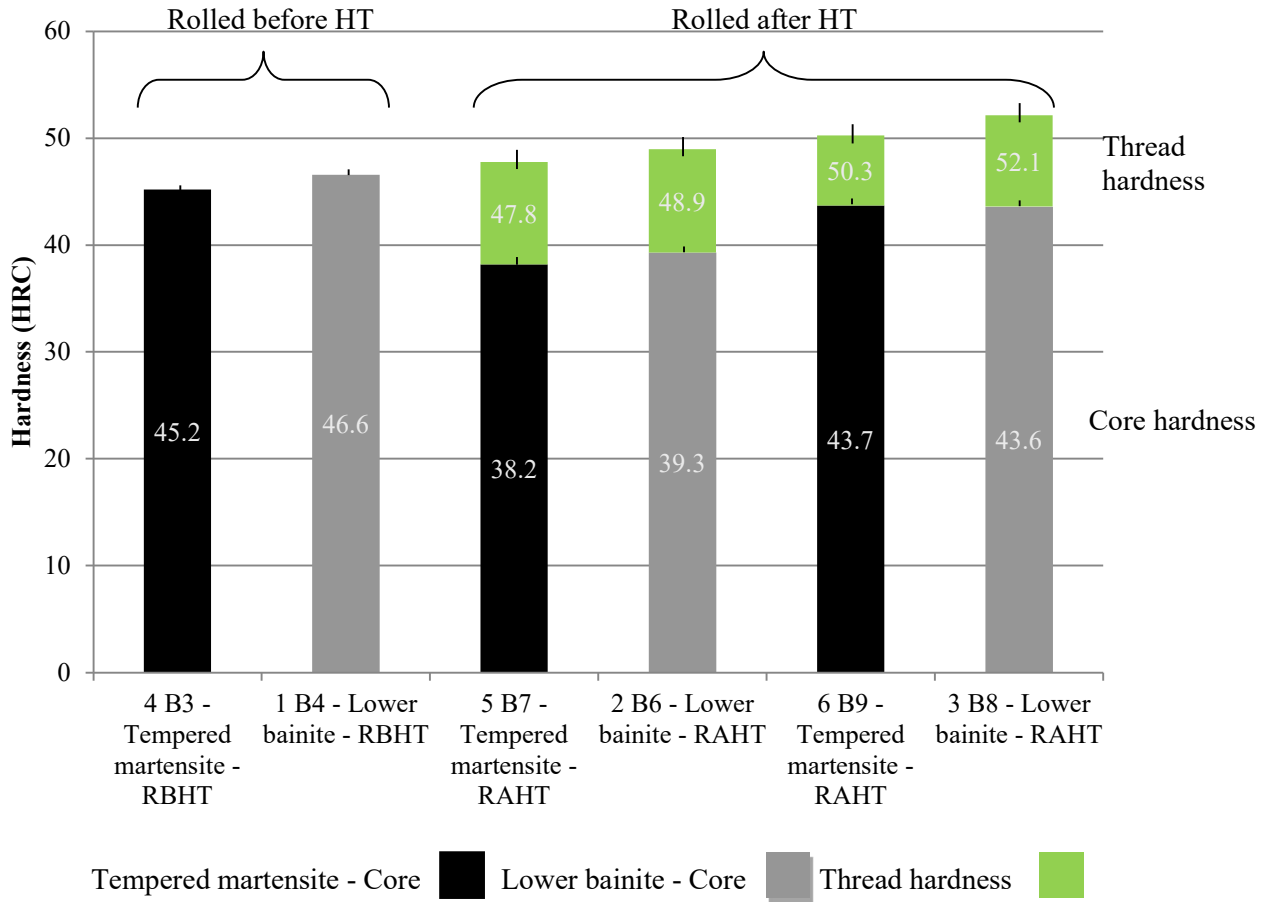


Figure 4.3: Core and thread hardness of rolled before and after HT of tempered martensite and lower bainite.



Figure 4.4: Machined tensile sample – modified ASTM E8-13a Fig. 8 Specimen 4.

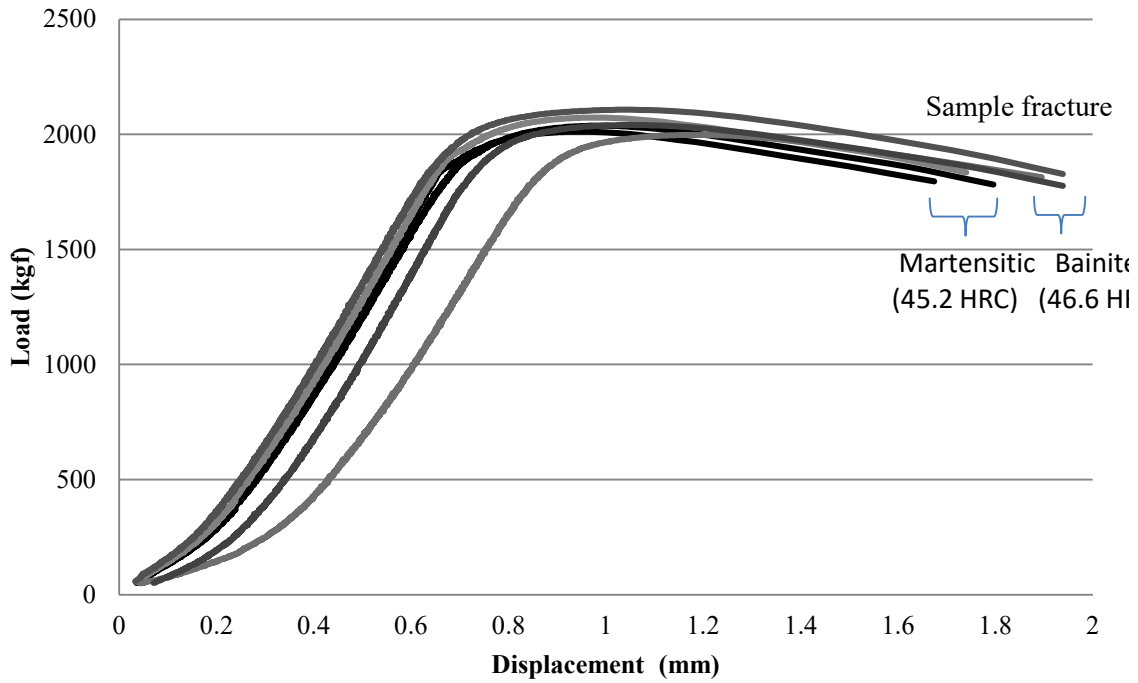


Figure 4.5: Tensile test curves show a trend towards greater ductility for bainitic samples – Thread rolling before heat treatment.

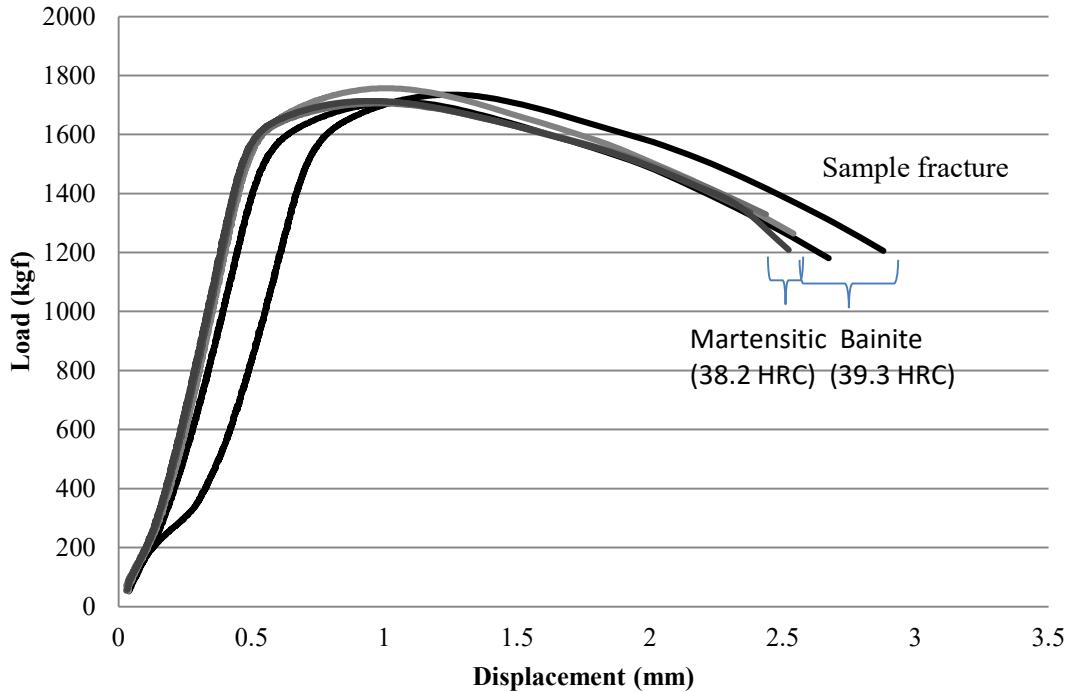


Figure 4.6: Tensile test curves show a trend towards greater ductility for bainitic samples - thread rolling after heat treatment (lower hardness).

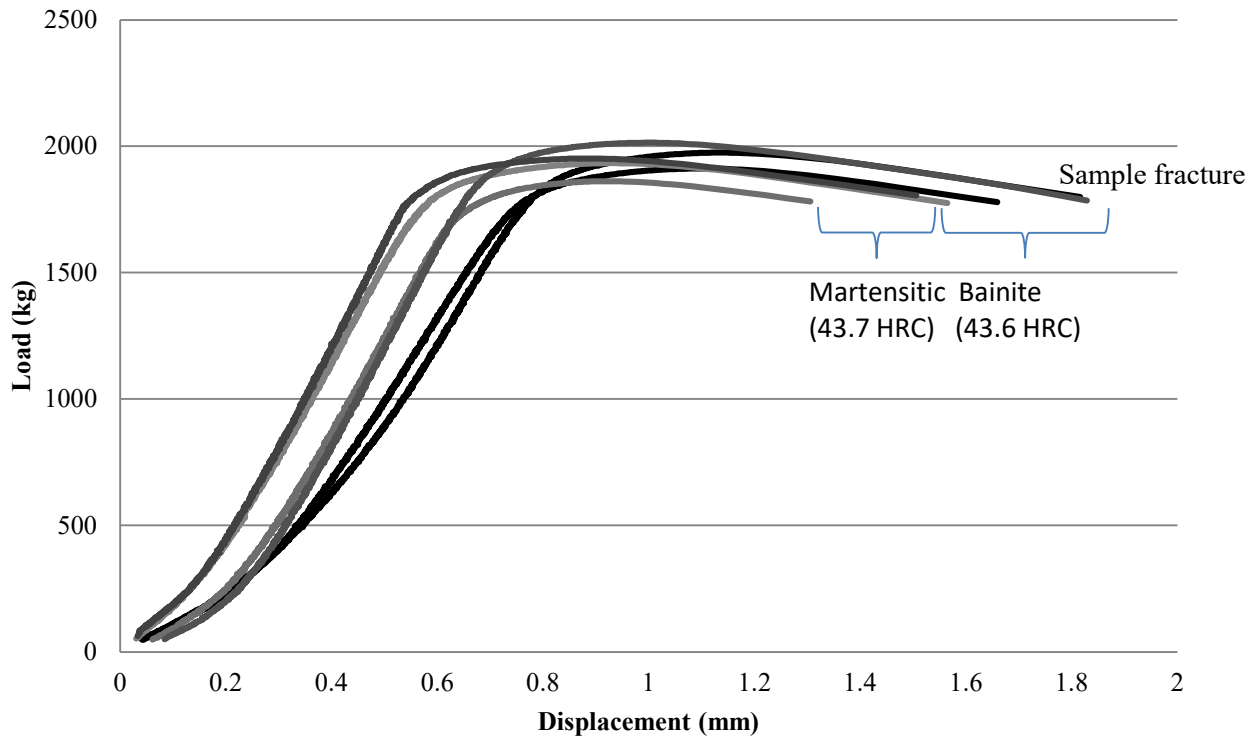


Figure 4.7: Tensile test curves show a trend towards greater ductility for bainitic samples - thread rolling after heat treatment (high hardness).

## **Chapter 5 : Publication Strategy**

The first objective of this research is to examine the effect of microstructure, specifically comparing martensite obtained by quenching and tempering to lower bainite obtained by austempering, on the susceptibility of steel fasteners to hydrogen embrittlement. The second objective is to examine the HE susceptibility of the same two microstructures with the added variable of altering the thread manufacturing sequence, specifically, rolling threads either before or after heat treatment. This thesis is based on two articles published in scientific journals reporting findings for each of the two objectives. Additional complementary results are given in Appendix.

### **5.1 Article 1 summary**

Saliby, F., Brahim, S., Rajagopalan, S., and Yue, S., *Hydrogen Embrittlement Susceptibility of Bainite for High Strength Steel Fasteners*. *Materials Performance and Characterization*, 2017. **6**(1): p. 462-471. [36]

This article, reproduced in Chapter 6, discusses the effect of microstructure on HE susceptibility. More precisely, HE susceptibility was slightly lower for bainite than martensite at moderate levels of hydrogen charging. At the most severe hydrogen charging condition, both microstructures were equally susceptible.

Contribution of authors: In this article, Fadi Saliby as the first author performed core hardness, HE susceptibility, fracture surface observations and wrote the manuscript. Exova laboratories performed the chemical and tensile evaluations. Sriraman Rajagopalan reviewed this manuscript. Salim Brahim and Steve Yue supervised the project and provided valuable input for this manuscript.

### **5.2 Article 2 summary**

Saliby, F., Brahim, S., Rajagopalan, S., and Yue, S., *Effect of Rolling after Heat Treatment on Hydrogen Embrittlement Susceptibility for High Strength Steel Fasteners*. *Materials Performance and Characterization*, 2020. **9**(1): p. 549-560. [37]

This article, reproduced in Chapter 7, discusses the effect on HE susceptibility of rolling the threads after heat treatment. More precisely, irrespective of the metallurgical structure (i.e., martensite or bainite), rolling the threads after heat treatment significantly reduced HE susceptibility.

Contribution of authors: In this article, Fadi Saliby performed HE susceptibility, microhardness evaluations and wrote the manuscript. Sriraman Rajagopalan performed X-ray diffraction analysis. Salim Brahim and Steve Yue supervised the project and reviewed this manuscript.

### **5.3 Complementary data**

Additional complementary data that were not published in the articles referred to in 5.1 and 5.2 are presented in Appendix I. These results consist of ISL data, microstructural, and fractographical examinations.

## **Chapter 6 : ARTICLE 1: Hydrogen Embrittlement Susceptibility of Bainite for High Strength Steel Fasteners**

### **6.1 Abstract**

Industrial fasteners of two different steel microstructures were investigated using incremental step load testing based on ASTM F1624, Standard Test Method for Measurement of Hydrogen Embrittlement Threshold in Steel by the Incremental Step Loading Technique. The microstructures consisted of tempered martensite and lower bainite. The purpose was to compare hydrogen embrittlement (HE) susceptibility at different hydrogen charging conditions. The results showed that lower bainite exhibited marginally lower HE susceptibility when tested under moderate hydrogen charging conditions (e.g., -1.0 V). At the most severe hydrogen charging potential of -1.2 V, both microstructures are equally embrittled. These results are explained by the differences in the transport and trapping kinetics of hydrogen in bainite as compared to martensite.

Keywords: metallurgy, steel, bainite, martensite, hydrogen, embrittlement, fracture, hardness, tensile, ductile

### **6.2 Introduction**

While the demand for stronger and lighter steels is increasing, hydrogen embrittlement (HE) becomes a greater concern to prevent catastrophic failures. Hydrogen is introduced into steel during manufacturing steps such as acid pickling and electroplating as well as during service from environmental effects such as corrosion [1]. An example of an application in which understanding and eliminating HE is important in the use of high strength fasteners is in the automotive industry to help reduce weight to meet more stringent average fuel economy standards (CAFE) [2].

HE is a time dependent (i.e., delayed) failure that occurs when the following three conditions are met: (i) hydrogen is present in the steel matrix, (ii) the material is susceptible (e.g., high strength), and (iii) there is a residual or applied stress on the part [3]. Take away any one of those conditions and failure will not occur.

It is generally understood that susceptibility to HE is directly related to material strength. Increasing strength has a first order effect on susceptibility. Material strength is fundamentally related to chemistry and microstructure.

High strength fasteners are typically quenched and tempered to obtain a tempered martensitic microstructure that combines strength, ductility, and toughness. Lower bainite, another steel microstructure, is very similar in many respects to tempered martensite; however, it has been reported that at equal hardness to tempered martensite, lower bainite has better ductility and toughness [1]. It has been assumed that these improved properties reduce HE susceptibility. The purpose of this investigation is to compare HE susceptibility of tempered martensite to lower bainite at equal strength.

### **6.3 Experimental Methodology**

The principal method used for this investigation was mechanical testing, specifically, incremental step load (ISL) testing, which is a modified form of slow strain rate testing [4]. The objective of ISL testing is to measure HE threshold stress under varying conditions of hydrogen exposure.

#### **6.3.1 Measuring threshold stress by mechanical testing**

The HE threshold stress is the minimum critical stress that causes failure for a given condition of hydrogen exposure. Below the threshold stress, failure does not occur.

Given that HE is a time dependent mechanism, ISL methodology combines stress and time. The applied step loading rates are significantly slower than standard tensile test method loading rates [5]. The loading rate must be sufficiently slow to permit hydrogen diffusion to the point of stress concentration. This leads to the formation of microcracks and fracture below nominal material strength.

The test is conducted in a four-point bending apparatus (Figure 6.1) with displacement control. Figure 6.2 shows a typical ISL testing curve showing the ISL.

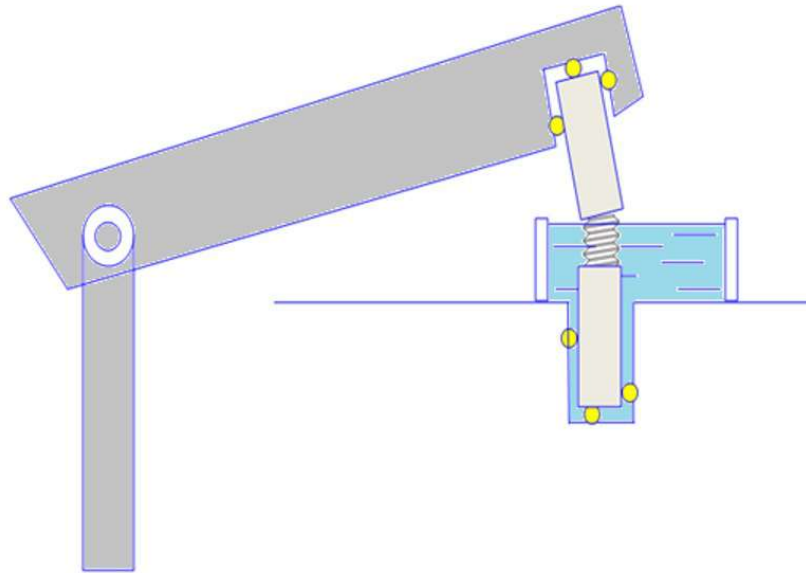


Figure 6.1: Incremental load testing apparatus.

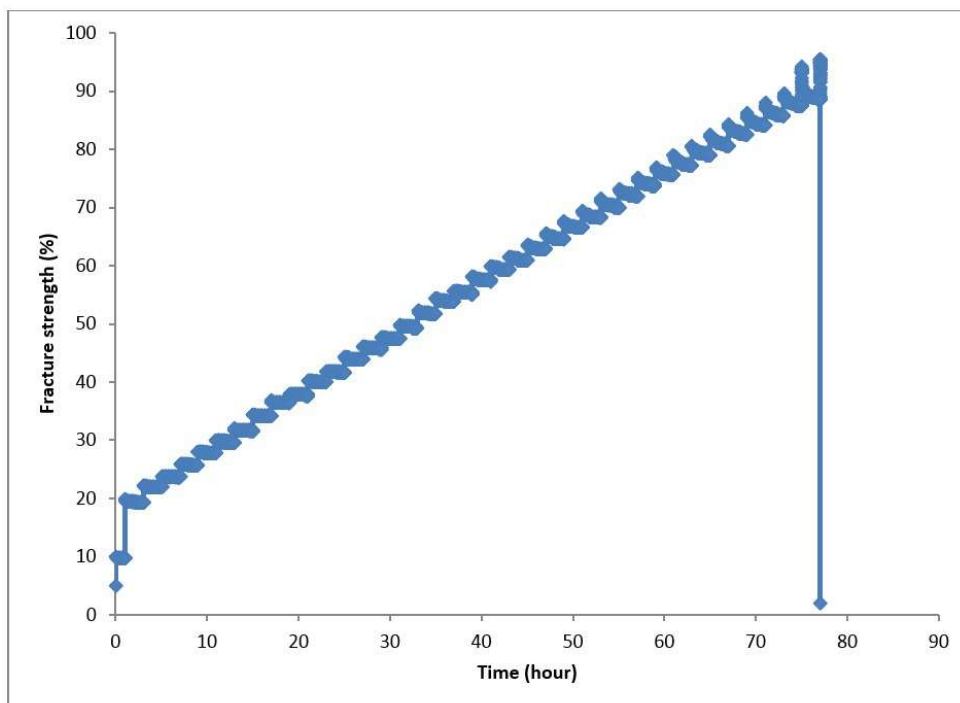


Figure 6.2: Example of an ISL testing curve.

### 6.3.2 Hydrogen charging conditions

Hydrogen embrittlement testing can be performed in air to evaluate the effect of residual hydrogen (i.e., internal HE) and under cathodic hydrogen charging conditions (i.e., environmental HE).

Cathodic charging consists of imposing a cathodic potential, which requires an inert anode and an external power source (potentiostat). The test environment is a 3.5 % sodium chloride solution. Hydrogen charging is accomplished by a three-electrode setup in which the anode is a platinum wire, the sample acts as cathode, and a saturated calomel electrode is used as a reference electrode. Figure 6.1 shows the experimental work station while Figure 6.3 describes the mechanism of hydrogen charging. The electrochemical reaction causes hydrogen gas evolution at the cathode due to electrolysis and hydrogen diffuses in the material by atomic hydrogen ( $H^+$ ) adsorption. The concentration of hydrogen ions absorbed by the sample surface increases with decreasing potentials from  $-0.9$  V to  $-1.2$  V. Electrode potential of  $-1.2$  V represents the most severe condition that replicates naturally occurring galvanic corrosion condition (e.g., pure zinc coating on steel).

Hydrogen embrittlement threshold experiments were carried out under five conditions for both materials, lower bainite and tempered martensite, as follows.

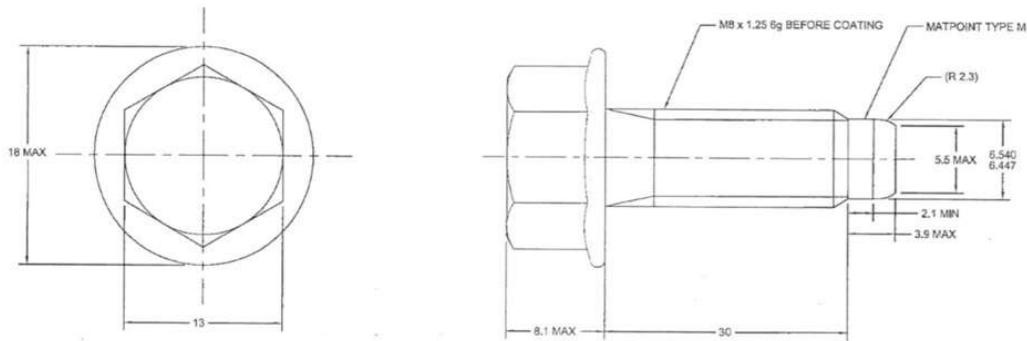
1. Fast fracture: four-point bending test using a rapid loading rate of 100 lbs/min.
2. ISL in air: four-point bending test using a slow step loading rate in air (2 %-2 h).
3. ISL at  $-0.9$  V: four-point bending test using a slow step loading rate (2 %-2 h) in a cathodic charging environment.
4. ISL at  $-1.0$  V: four-point bending test using a slow step loading rate (2 %-2 h) in a cathodic charging environment.
5. ISL at  $-1.2$  V: four-point bending test using a slow step loading rate (2 %-2 h) in a cathodic charging environment



## 6.4 Material Conditions

Screw samples, M8-1.25 by 30 mm, were produced by an automotive fastener manufacturer using AISI 8640 nickel-chromium-molybdenum steel alloy from the same coil.

Figure 6.4 shows the schematic and a photograph of an actual finished product. Samples were coated with water soluble oil to prevent corrosion. Two different heat treatment processes were applied to obtain tempered martensite and lower bainite at a target hardness of 45 Rockwell C (HRC). The heat treatment cycle to obtain each microstructure is shown in Figure 6.5. The tempered martensite samples were austenitized at 865°C, oil quenched, and then tempered at 432°C. The lower bainite samples were austenitized at 885°C and quenched in a salt bath at 364°C to achieve isothermal transformation. Resulting microstructures are shown in Figure 6.6. The microstructures were indistinguishable at magnification up to 7,000×. Sample chemical compositions are given in Table 6.1. The analysis was performed by combustion analysis (carbon, sulfur, and hydrogen) and inductively coupled plasma (ICP) spectroscopy (remaining elements).



(a)



(b)

Figure 6.4: Drawing of the screw (a). Actual supplied sample (b).

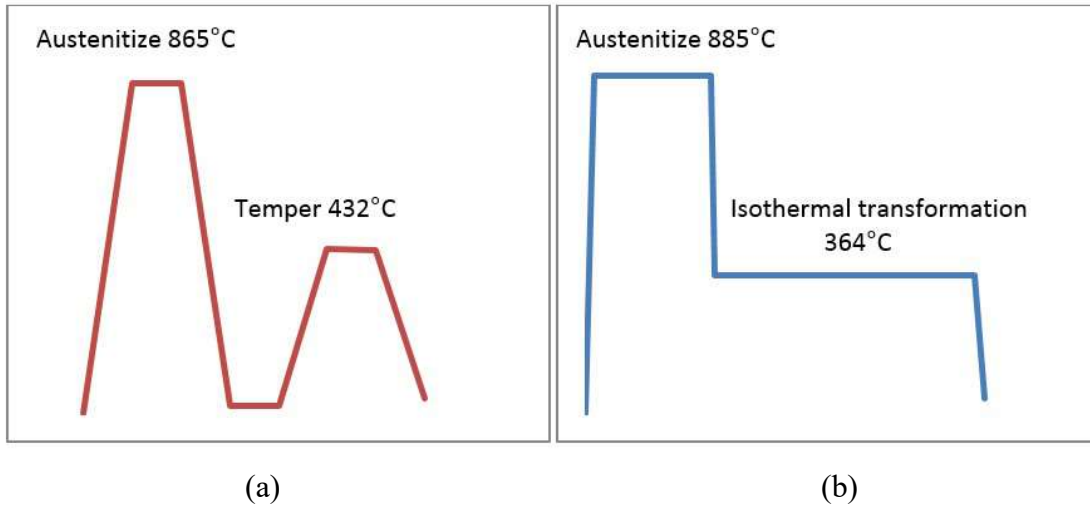


Figure 6.5: Heat treatment cycles for tempered martensite (a) and lower bainite (b).

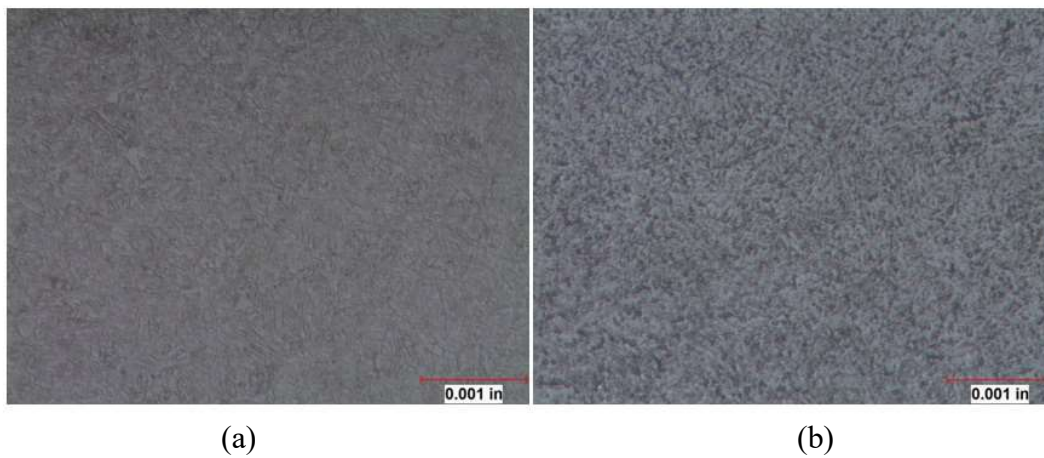


Figure 6.6: Tempered martensite (a) and lower bainite (b) microstructure (500X / Nital 2%). The chemical analysis confirmed that both sets of samples were AISI 8640 with identical chemistry. Bainitic samples contained a hydrogen concentration five times greater than martensitic samples (0.6 versus 3.4 ppm).

Figure 6.7 shows the machined micro tensile specimen extracted from a fastener.



Figure 6.7: Machined tensile sample – modified ASTM E8-13a (Standard Test Methods for Tension Testing of Metallic Materials) [5] Fig. 8 Specimen 4

## 6.5 Results

The chemical analysis confirmed that the bainitic samples contained hydrogen concentration five times greater than martensitic samples (0.6 versus 3.4 ppm), see Table 6.1.

Table 6.1: Chemical composition

Material ID	Microstructure	% C	% Cr	% Mn	% Mo	% Ni	% P	% S	% Si	H (ppm)
1	Tempered Martensite	0.39	0.45	0.80	0.15	0.45	0.007	0.012	0.20	0.6
2	Lower Bainite	0.40	0.44	0.80	0.15	0.44	0.006	0.014	0.20	3.4
AISI 8640 Requirement		0.38-0.43	0.40-0.60	0.75-1.00	0.15-0.25	0.40-0.70	0.035 Max	0.040 Max	0.15-0.35	-

**Abbreviation:** max, maximum.

This difference is attributed to the different heat treatments processes. An important note to make is that the total measured hydrogen includes diffusible and trapped hydrogen, i.e., hydrogen that plays a role in HE and hydrogen that does not affect HE, respectively [7]. The tempering of martensite is performed at a higher temperature in atmosphere as compared to austempering of lower bainite, which is performed in a salt bath. The higher tempering temperature facilitates outward hydrogen diffusion [8]. Also, austempering in molten salt may hinder outward hydrogen diffusion.

Figure 6.8 shows the load versus displacement curves. The small sample size did not allow the use of an extensometer to measure strain. The average tensile strength and reduction of area for both tempered martensite and lower bainite samples are given in Table 6.2. Despite having slightly higher hardness, lower bainite achieved significantly greater reduction of area (27.4 versus 21.2 %).

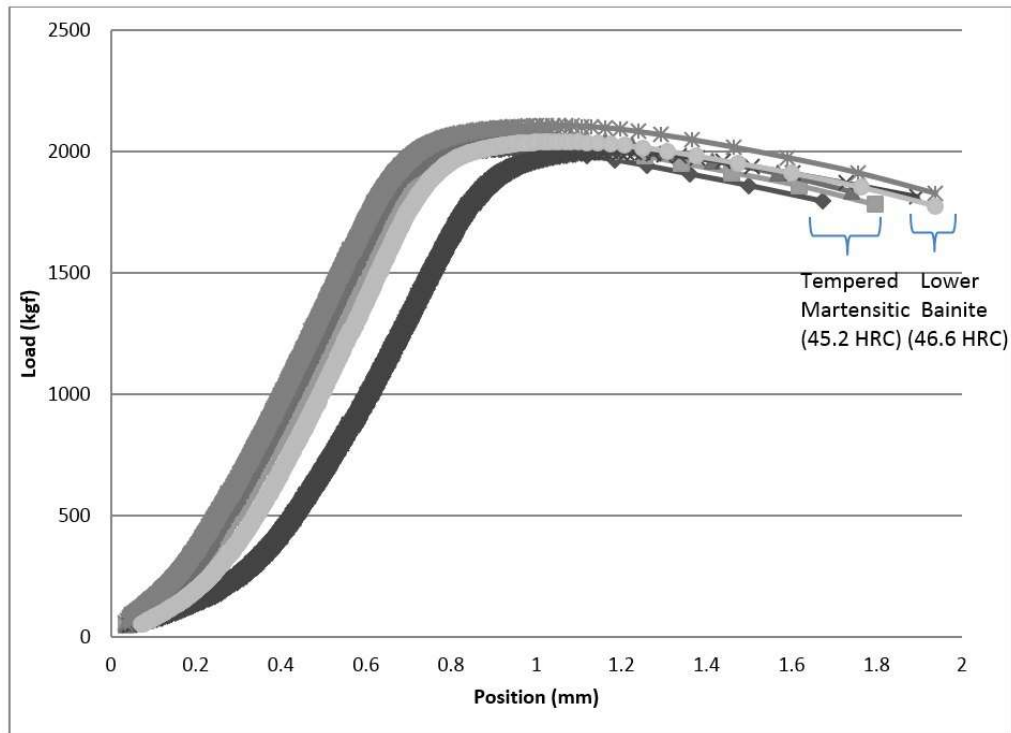


Figure 6.8: Load vs. displacement curves for tempered martensite and lower bainite.

Figure 6.9 illustrates the average threshold loads at each of the five test conditions. A small drop in threshold load between fast fracture and ISL in air is attributed to residual hydrogen. Testing under cathodic charging conditions showed a significant drop in threshold loads for both microstructures. The greatest drop occurs at  $-1.2\text{V}$ .

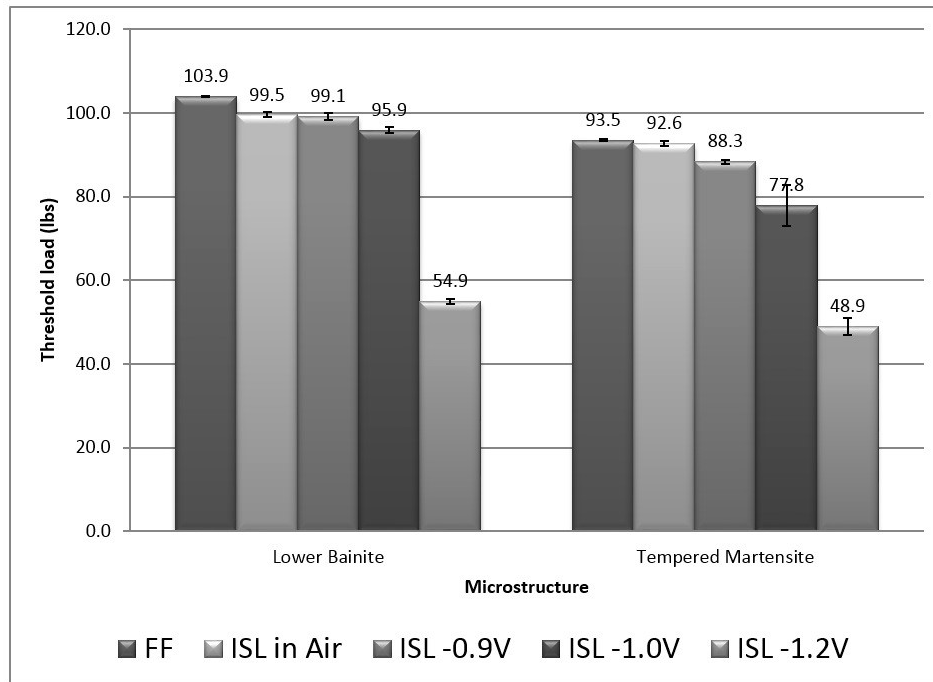


Figure 6.9: Bainite and martensite threshold loads at different cathodic charging conditions.

Figure 6.10 shows the normalized NFS% results. The results are plotted as threshold curves showing a ductile to brittle transition with increasing hydrogen charging [9]. The transition for lower bainite occurs further to the left, which signifies that the structures become brittle with higher concentrations of hydrogen compared to tempered martensite. The difference is most notable at the  $-1.0\text{ V}$  condition (bainite: 92 % versus martensite: 83 %). At  $-0.9\text{ V}$ , the charging condition was low and caused a comparable 5 % drop for both microstructures. At  $-1.2\text{ V}$ , the charging condition was aggressive and led to a similar drop (bainite: 53 % versus martensite: 52 %).

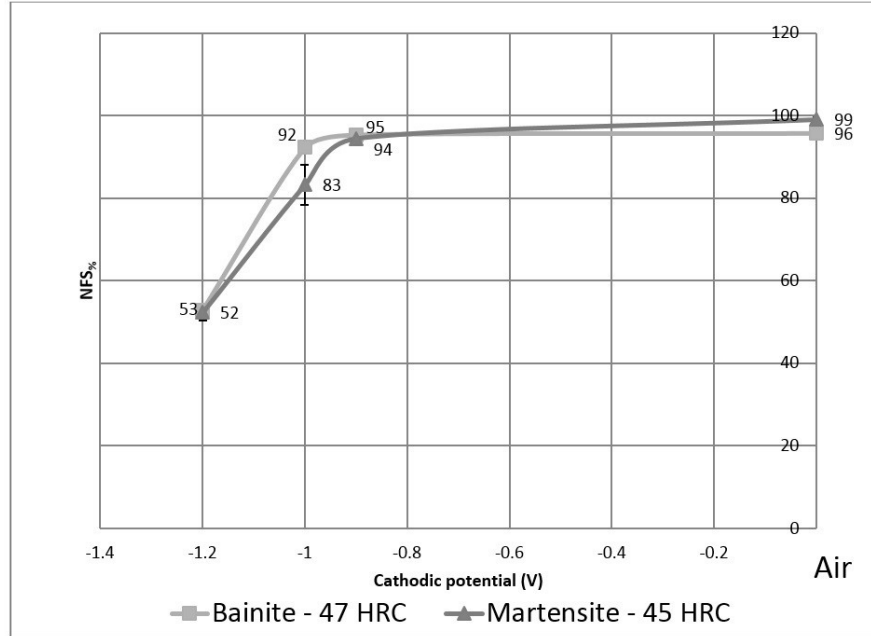


Figure 6.10: Percent notch fracture strength (NFS%) versus cathodic potential.

To help differentiate both microstructures, optical, tint etching, and scanning electron microscope methods were utilized. However, the microscale differences between both microstructures were not identified.

## 6.6 Discussion

Threshold testing showed lower bainite achieved higher threshold loads under cathodic charging even though lower bainite had slightly higher hardness and strength over tempered martensite. In other words, lower bainite has a lower HE susceptibility under moderate charging condition. Lower bainite also had improved ductility. Other studies have shown that at hardness above  $\geq 450$  HB (approximately 47 HRC), lower bainite exhibits higher ductility than tempered martensite [10,11]. The higher HE threshold may be correlated to the higher ductility of lower bainite over tempered martensite. As the material is more ductile, dislocations emission increases and grain decohesion decreases. An increase in dislocation emission delays cleavage damage [12]. Hydrogen will hinder dislocation emission; however, as the dislocation to hydrogen concentration ratio increases (more ductile materials), less will the effect of pinning by hydrogen be felt.

Another hypothesis that explains the lower HE susceptibility of lower bainite may be explained by variations in hydrogen transportation and trapping behaviors related to the

microstructure. These findings are consistent with previous studies [8]. Hydrogen trapping is classified as reversible (e.g., dislocations, vacancies) and irreversible (e.g., carbides, grain boundaries). Literature states diffusible and reversible hydrogen causes embrittlement; however, hydrogen in irreversible traps does not [13,14]. Others [15] reported that the lower bainite contained finer and more uniformly distributed carbides, a higher amount of dissolved carbon in bainitic ferrite, and fine bainitic ferrite grains. Results of this current study showed that lower bainite microstructures were less embrittled for the potential reason that more irreversible hydrogen trapping could have occurred. When forming lower bainite, small carbides particles are dispersed and they are found at the ferrite and austenite interface. Further precipitation of carbides can occur during the martensitic transformation. In the present case, the difference in carbide shape, size, distribution, and composition between both microstructures could be affecting hydrogen pinning and trapping. The experimental investigation of precipitates was beyond the scope of this research. This will be reserved for future work.

Future work includes transmission electron microscopy analysis to help differentiate and validate the microstructure, diffusion analysis by permeation studies, thermal desorption to analyze hydrogen trapping states, and evaluating hydrogen pickup/loss during heat treatments.

## **6.7 Conclusions**

ISL testing was used to evaluate the effect of hydrogen charging conditions on HE susceptibility. This study showed that a lower bainite microstructure had a slightly lower HE susceptibility at moderate hydrogen charging condition. At highest and lowest charging conditions ( $-0.9$  V and  $-1.2$  V), both microstructures exhibited similar behavior.

Lower bainite's improved NFS%, increased ductility, and ability to be precharged with hydrogen shows that this microstructure might have a slight advantage over tempered martensite for fasteners application.

It should be cautioned that lower bainite showed only a marginal improvement and is still very susceptible. HE behavior should not be the deciding factor in selecting this microstructure.

## 6.8 References

1. Raymond, L., “Evaluation of Hydrogen Embrittlement,” *ASM Handbook, Volume 13, Corrosion*, ASM International, Materials Park, OH, 1987, pp. 283–290.
2. “CAFE - Fuel Economy,” NHTSA, 2016, [Online]. Available: <https://web.archive.org/web/20170118220646/https://www.nhtsa.gov/laws-regulations/corporate-average-fueleconomy> (accessed 18 Jan. 2017).
3. Craig, B., “Hydrogen Damage,” *ASM Metals Handbook, Ninth Edition, Volume 13A, Corrosion*, ASM International, Materials Park, OH, 1987, pp. 163–171.
4. ASTM F1624-12, *Standard Test Method for Measurement of Hydrogen Embrittlement Threshold in Steel by the Incremental Step Loading Technique*, ASTM International, West Conshohocken, PA, 2012, [www.astm.org](http://www.astm.org)
5. ASTM E8/E8M-16, *Standard Test Methods for Tension Testing of Metallic Materials*, ASTM International, West Conshohocken, PA, 2016, [www.astm.org](http://www.astm.org)
6. Dafft, E. G., Bohnenkamp, K., and Engell, H. J., “Investigations of Hydrogen Evolution Kinetics and Hydrogen Absorption by Iron Electrodes During Cathodic Polarization,” *Corros. Sci.*, Vol. 19, No. 7, 1979, pp. 591–612, [https://doi.org/10.1016/S0010-938X\(79\)80061-X](https://doi.org/10.1016/S0010-938X(79)80061-X)
7. Brahim, S., *Fundamentals of Hydrogen Embrittlement in Steel Fasteners*, IBECA Technologies Corp., Montreal, 2014, pp. 1–23, <https://web.archive.org/web/20170227150732/https://www.boltcouncil.org/files/HydrogenEmbrittlementInSteelFastenersBrahimi.pdf> (accessed 27 Feb. 2017).
8. Fleurentin, A., Creus, J., and Feaugas, X., “Impact de la Structure Métallurgique sur le Chargement et la Désorption Naturelle de L’Hydrogène dans un acier (37Cr4) Traite à 1250 MPa,” *Cetim*, Paris, 2013.
9. ASTM F1940-07a, *Standard Test Method for Process Control Verification to Prevent Hydrogen Embrittlement in Plated or Coated Fasteners*, ASTM International, West Conshohocken, PA, 2014, [www.astm.org](http://www.astm.org)

10. Totten, G. E., *Steel Heat Treatment: Metallurgy and Technologies*, *Steel Heat Treatment Handbook, Second Edition*, CRC Press, Boca Raton, FL, 2006, p. 409.
11. Tu, M.-Y., Hsu, C.-A., Wang, W.-H., and Hsu, Y.-F., “Comparison of Microstructure and Mechanical Behavior of Lower Bainite and Tempered Martensite in JIS SK5 Steel,” *Mater. Chem. Phys.*, Vol. 107, Nos. 2–3, 2008, pp. 418–425, <https://doi.org/10.1016/j.matchemphys.2007.08.017>
12. Milne, I., Ritchie, O., and Karihaloo, B., *Comprehensive Structural Integrity*, Elsevier, Amsterdam, Netherlands, 2003, p. 5232.
13. Grabke, H. J. and Riecke, E., “Absorption and Diffusion of Hydrogen in Steels,” *Mater. Tehnol.*, Vol. 34, No. 6, 2000, pp. 331–342.
14. Lупpo, M. I. and Ovejero-Garcia, J., “The Influence of Microstructure on the Trapping and Diffusion of Hydrogen in a Low Carbon Steel,” *Corros. Sci.*, Vol. 32, No. 10, 1991, pp. 1125–1136, [https://doi.org/10.1016/0010-938X\(91\)90097-9](https://doi.org/10.1016/0010-938X(91)90097-9)
15. Sajjadi, S. A. and Zebarjad, S. M., “Isothermal Transformation of Austenite to Bainite in High Carbon Steels,” *J. Mater. Process. Technol.*, Vol. 189, Nos. 1–3, 2007, pp. 107–113, <https://doi.org/10.1016/j.jmatprotec.2007.01.011>

## **Chapter 7 : ARTICLE 2: Effect of Rolling after Heat Treatment on Hydrogen Embrittlement Susceptibility for High Strength Steel Fasteners**

### **7.1 Abstract**

Steel fasteners comprising two different metallurgical structures were investigated for hydrogen embrittlement (HE) susceptibility by incremental step load testing. The metallurgical structures examined consisted of tempered martensite obtained by quenching and tempering and lower bainite obtained by austempering. It has been shown that lower bainite exhibits marginally lower HE susceptibility when tested under moderate hydrogen charging conditions (e.g.,  $-1.0$  V). At the most severe hydrogen charging potential of  $-1.2$  V, both microstructures are equally embrittled. The current paper examines the effect of the sequence of the fabrication process, specifically the effect of rolling the threads before and after heat treatment (i.e., quenching and tempering or austempering). The results show irrespective of the metallurgical structure, rolling the threads after heat treatment causes a significant decrease in HE susceptibility. These findings are attributed to the presence of high dislocation density when thread rolling is performed on hardened parts as a final manufacturing step.

Keywords: metallurgy, steel, bainite, martensite, hydrogen, embrittlement, fracture, hardness, ductile, thread rolling

### **7.2 Introduction**

Hydrogen embrittlement (HE) causes sudden failures of components during service. This embrittlement mechanism affects steels and other metal alloys. Hydrogen may be absorbed during manufacturing steps as well as during corrosion.<sup>1</sup> HE occurs in materials that are susceptible to hydrogen damage (e.g., high strength steel) while subjected to tensile stress (i.e., from service load or residual stress) and are exposed to a source of hydrogen.<sup>2,3</sup> Susceptibility to HE is directly related to the material condition, notably strength, which is a function of chemistry and microstructure.<sup>3</sup>

The objective of this study is to investigate the effects of microstructure on the susceptibility of steel fasteners to HE. More precisely, the study compares two microstructures,

traditional quenched and tempered martensite and lower bainite obtained by austempering. Tempered martensite is the microstructure typical in high strength fasteners. Lower bainite, a microstructure similar to tempered martensite, is being introduced in fasteners to achieve an acceptable amount of ductility and toughness at strength levels greater than the standard quenched and tempered fasteners (e.g., 1,400–1,800 MPa). At equal strength/hardness, lower bainite has been shown to exhibit higher ductility and toughness than tempered martensite.<sup>1</sup>

Fastener threads are manufactured by cold forming (i.e., thread rolling) or machining (i.e., cutting). The majority of industrial fasteners undergo thread rolling before heat treatment (RBHT). This is the most cost-effective manufacturing sequence. However, in bolted joint applications where dynamic service loads can initiate fatigue, threads are typically rolled after heat treatment (RAHT). Critical engine fasteners in the automotive industry and all aerospace fasteners fall into this category. RAHT introduces compressive residual stresses in the threads and increases fatigue life.<sup>4,5</sup> It has been assumed that improved mechanical properties of bainite, notably higher ductility and toughness, lower its HE susceptibility when compared to martensite. The findings of this study presented in a separate publication show this assumption to be true.<sup>6</sup> This paper examines the effect of RAHT on HE susceptibility.

### **7.3 Experimental Method**

The purpose of this evaluation is to compare HE susceptibility both with and without the introduction of hydrogen by cathodic hydrogen charging. The primary test method utilized is incremental step load (ISL) testing. The test is conducted in a four-point bending apparatus (see Figure 7.1) with displacement control on a notched sample. The apparatus was manufactured by Fracture Diagnostics Inc. The HE threshold stress is measured<sup>7</sup> under varying conditions of hydrogen exposure. The HE threshold stress is defined as the minimum critical stress that causes failure for a given condition of hydrogen exposure.

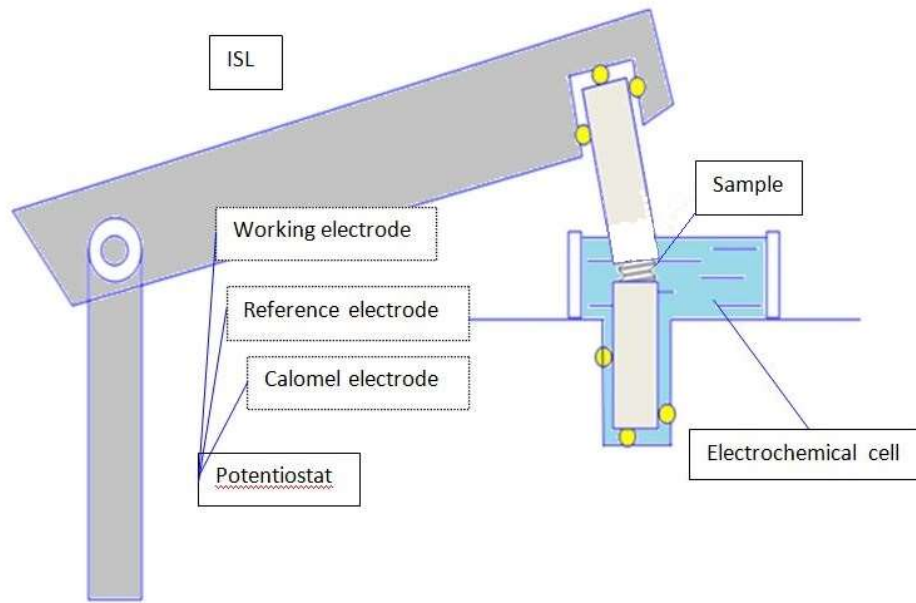


Figure 7.1: Schematic of incremental load testing apparatus.

Hydrogen embrittlement testing was performed in air or under cathodic hydrogen charging conditions. When the test is performed in air, only the effect of residual internal hydrogen is evaluated. Under cathodic hydrogen charging conditions, the effect of additional environmental hydrogen is evaluated. This approach consists of imposing a cathodic potential in a 3.5 % by weight sodium chloride solution. The sample is evaluated while immersed in this solution. The electrochemical reaction causes hydrogen gas evolution and adsorption onto the surface of the metal. Atomic hydrogen is then absorbed by the material. By varying the imposed potential between  $-0.8$  V and  $-1.2$  V versus a saturated calomel electrode, the concentration of hydrogen absorbed by the sample is varied. As the imposed potential is decreased, the concentration of hydrogen absorbed is increased.

The experiments are performed to measure threshold stress, which is defined as the stress below which failure will not occur for a given amount of hydrogen. The experiments are performed as follows.

(1) Fast fracture (FF): 4-point bending test using a rapid loading rate of 100 lbs/min to establish the baseline strength. Given the speed of the test (i.e., 1–2 minutes), hydrogen does not have an effect.

- (2) ISL in air: 4-point bending test using a slow step loading rate in air (2 %–2 h) to isolate any effect of residual hydrogen that may have been present in the material.
- (3) ISL at –0.8 V, –1.0 V, and –1.2 V: 4-point bending test using a slow step loading rate (2 %–2 h) in a cathodic charging environment to measure the threshold strength under varying hydrogen charging conditions.

The effect of hydrogen on the mechanical properties at a given hydrogen charging condition is quantified by the notch fracture strength (NFS), which is described by the following expression for cathodic charging potential of –1.2 V:

$$NFS_{\% -1.2 V} = \frac{ISL_{-1.2 V}}{FF} \quad (1)$$

where:

$NFS_{\% -1.2 V}$  is the NFS at a –1.2 V hydrogen charging condition;

$ISL_{-1.2 V}$  is the fracture load at a –1.2 V hydrogen charging condition; and

FF is the baseline FF load in air.

When the test is performed at a sufficiently slow loading rate resulting in a lowest invariant load,  $NFS_{\%xxV}$  is taken to represent the HE threshold. In this study, the loading protocol of 2 % increment and held for 2-hour steps was used to obtain the lowest invariant load.

## 7.4 Material conditions

Screw samples, M8-1.25 by 30 mm, were fabricated by 2 different fastener manufacturers from American Iron and Steel Institute (AISI) 8640 nickel-chrome-molybdenum steel alloy. The samples were then heat treated (i.e., quench and tempered or austempered). The tempered martensite samples were austenitized at 865°C, the oil quenched and then tempered at 432°C. The lower bainite samples were austenitized at 885°C and quenched in a salt bath at 364°C to achieve isothermal transformation (see Figure 7.2).<sup>6</sup> The microstructures were indistinguishable (see Figure 7.3).<sup>6</sup> At higher magnification under the scanning electron microscope, differences between both microstructures were not evident (see Figure 7.3).

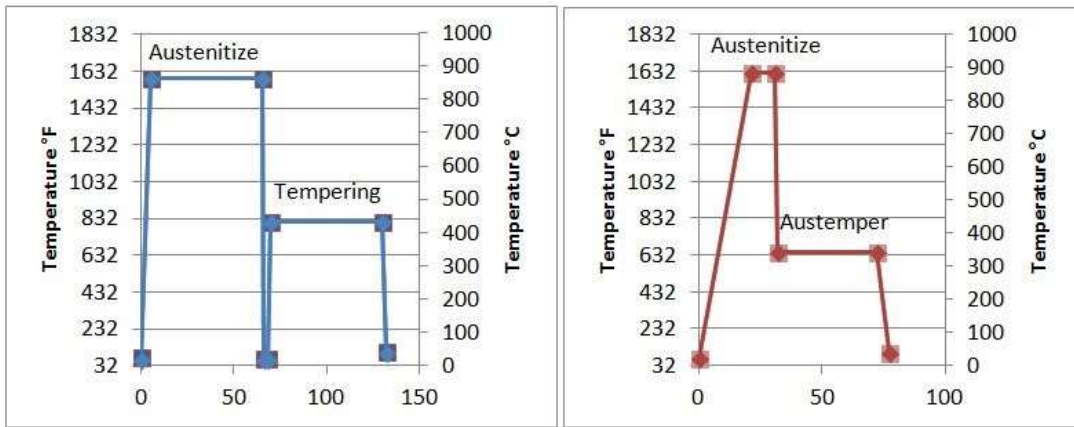


Figure 7.2: Heat treatment of tempered martensite (left) and lower bainite (right).

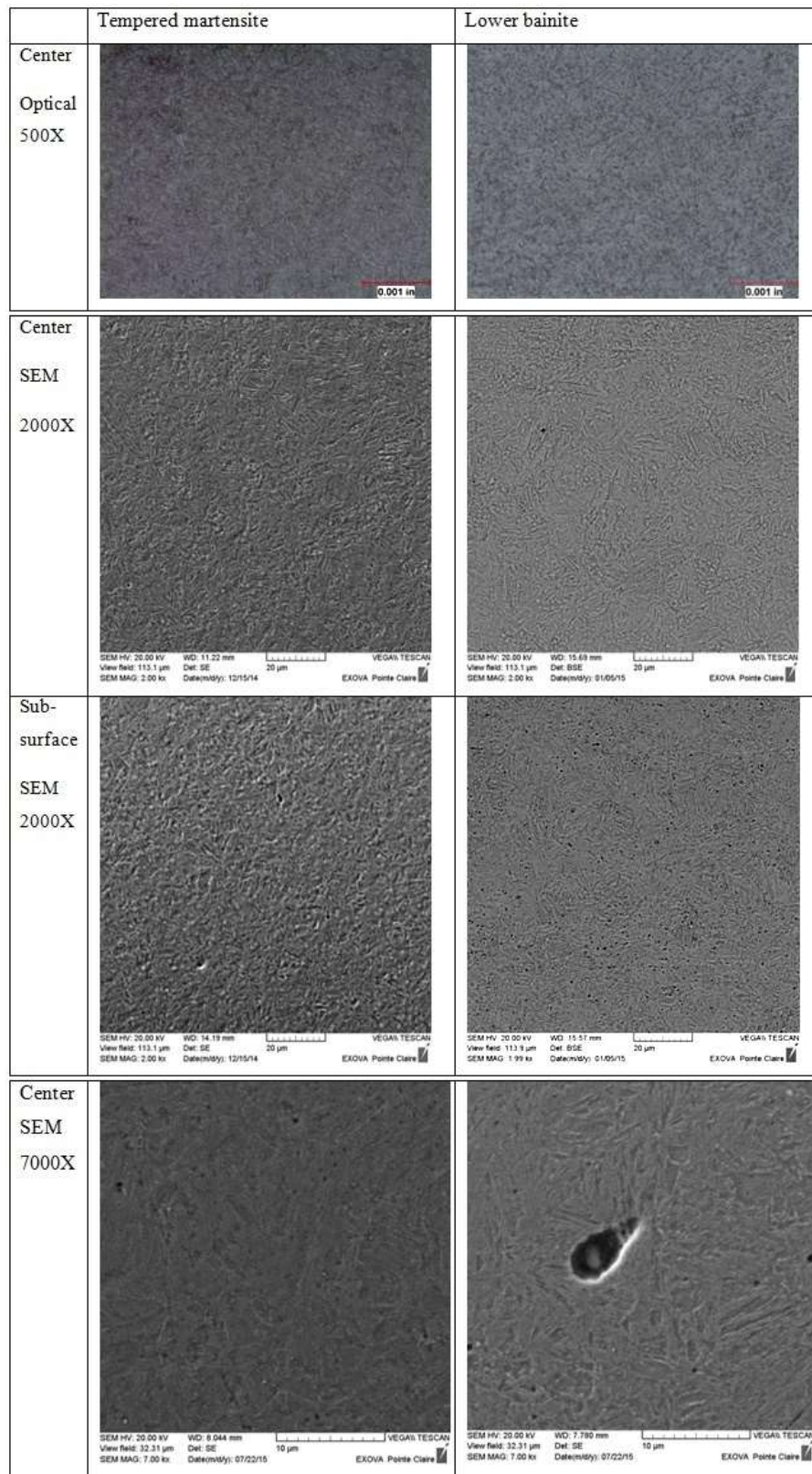


Figure 7.3: Tempered martensite (left) and lower bainite (right) microstructures (Nital 2 %).

Retained austenite was not observed optically during metallographic evaluations on either microstructure. Also, X-ray diffraction (XRD) analysis did not reveal any retained austenite (see Figure 7.4). The XRD patterns of all samples showed body centered cubic iron peaks typical of martensitic or bainitic microstructure. The 110, 200, and 211 peaks were clearly resolved. XRD was performed with a Bruker Discover D8 - X-ray diffractometer equipped with a 2D VANTEC 500 detector. The anode is a cobalt tube with a 1.78 Angstrom wavelength.

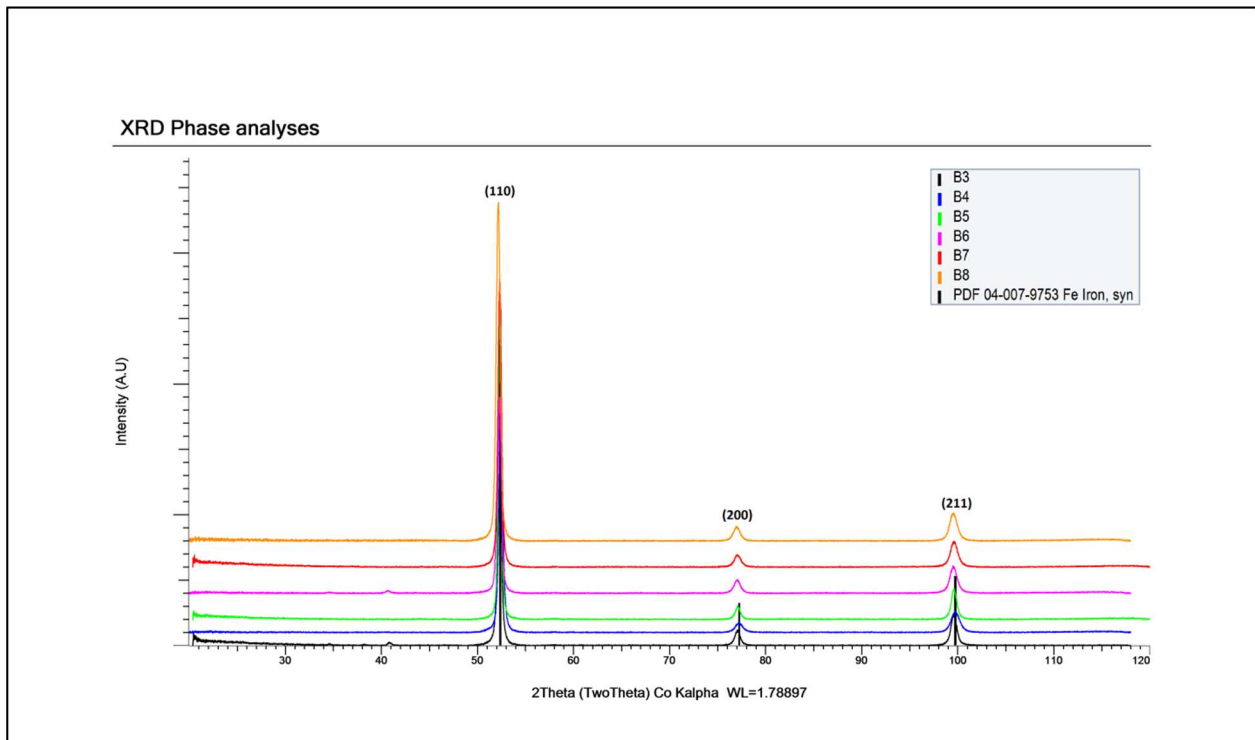


Figure 7.4: XRD on both martensite (B3, B5, B7) and lower bainite (B4, B6, B8) microstructures.

The chemical composition of the material is given in Table 7.1. The composition was determined by combustion analysis (carbon, sulfur, and hydrogen) and inductively coupled plasma (ICP) spectroscopy (remaining elements).<sup>6</sup>

The chemical analyses of all 4 sample groups confirmed that the materials complied with AISI 8640 chemistry. Hydrogen concentration in bainitic samples was higher than martensitic samples. This difference is attributed to the tempering condition for tempered martensite (432°C) versus the austempering temperature for bainite (364°C) in molten salt. The higher tempering temperature in atmosphere promotes hydrogen desorption.

The material conditions of the samples are given in Table 7.2.

The average tensile strength and reduction of area for both tempered martensite and lower bainite samples are given in Table 7.3. At similar or higher hardness, lower bainite achieved a slightly greater reduction of area.

Table 7.1: Chemical composition for each group of samples

Material ID	Microstructure	% C	% Cr	% Mn	% Mo	% Ni	% P	% S	% Si	H, ppm
1 B4	Lower Bainite	0.40	0.44	0.80	0.15	0.44	0.006	0.014	0.20	3.4
2 B8		0.44	0.50	0.95	0.18	0.49	0.012	0.002	0.22	2.5
3 B3	Tempered Martensite	0.39	0.50	0.80	0.15	0.44	0.007	0.012	0.20	0.6
4 B9		0.44	0.50	0.94	0.18	0.49	0.011	0.002	0.22	1.9
AISI 8640 Requirement		0.38-0.43	0.40-0.60	0.75-1.00	0.15-0.25	0.40-0.70	0.035 Max	0.040 Max	0.15-0.35	-

Table 7.2: Material conditions, including microstructure and thread rolling

Material ID	Microstructure	Nominal hardness (HRC)	Thread condition
1 B4	Lower bainite	44	RBHT
2 B8			RAHT
3 B3	Tempered martensite		RBHT
4 B9			RAHT

Table 7.3: Mechanical properties

Material ID	Microstructure	Hardness (Mid-radius HRC)	Hardness (Sub surface converted from HV0.1 to HRC) at 0.002"	Tensile Strength, MPa	Elongation, %	Reduction of area, %
1 B4	Lower Bainite	46.6 ± 0.3	46.9 ± 1.0	1,562 ± 12	19.4 ± 3.8	27.4 ± 4.4
2 B8		43.6 ± 0.2	52.1 ± 1.9	1,440 ± 15	13.7 ± 1.8	31.8 ± 1.1
3 B3	Tempered Martensite	45.2 ± 0.4	47.4 ± 0.7	1,521 ± 6	12.0 ± 1.7	21.2 ± 0.3
4 B9		43.7 ± 0.5	50.3 ± 1.3	1,456 ± 10	17.0 ± 2.8	27.8 ± 3.2

However, lower bainite showed lower % elongation in some conditions that can be attributed to the shape of the custom tensile specimen. It is possible that lower bainite is not more ductile than tempered martensite in all conditions.

## **7.5 Results**

### **7.5.1 Effect of rolling threads on NFS%**

In previous work,<sup>6</sup> a significant drop of the NFS% for both microstructures was observed at  $-1.2$  V. In that previous case, rolling of threads was performed before heat treatment (see Figure 7.5). A slight NFS% improvement was observed at a charging condition of  $-1.0$  V. In this study, RAHT showed no significant loss of fracture strength irrespective of microstructure. Figure 7.6 compares the NFS% values for bainite rolled before and after heat treatment at a similar hardness. At the most severe hydrogen charging condition of  $-1.2$  V, NFS% values were significantly improved in the RAHT condition (89 % versus 53 %). Figure 7.7 shows a similar behavior when comparing tempered martensite samples: at the most severe H charging condition of  $-1.2$  V, NFS% values were significantly improved in the RAHT condition (90 % versus 52 %). For both microstructures, no discernible ductile to brittle transition with increasing hydrogen charging<sup>8</sup> was observed in the RAHT condition (as seen graphically in Figure 7.8). At the most severe charging condition, a drop of 10 % and 11 % was observed with RAHT. The ductile to brittle transition was evident for samples RBHT (as seen graphically in Figure 7.5).

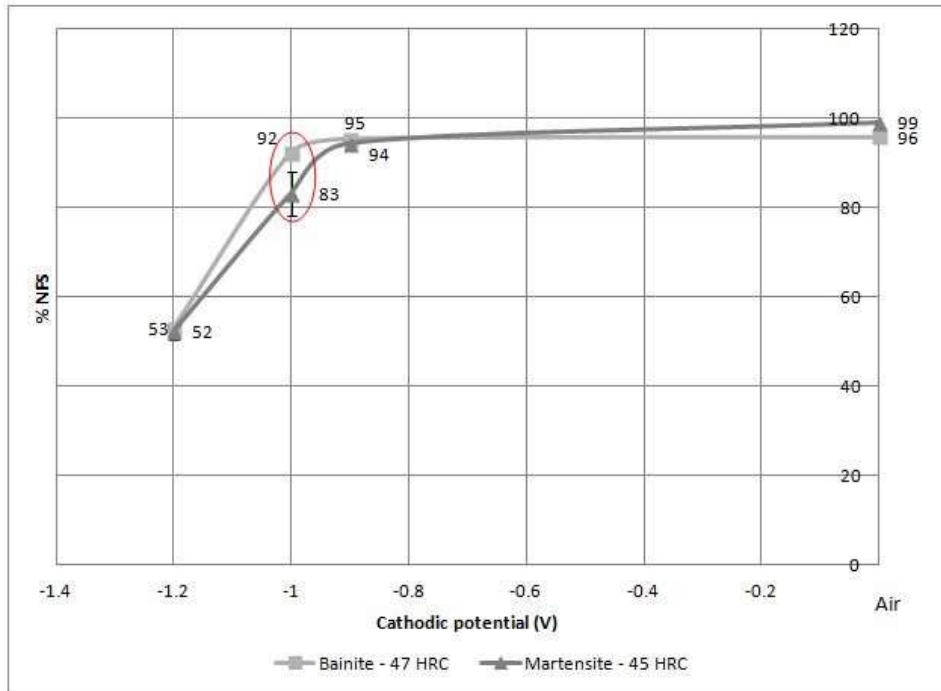


Figure 7.5: NFS% drop with increasing cathodic potential for both martensite and bainite when RBHT. Bainite showed less of an NFS% drop at -1.0 V.

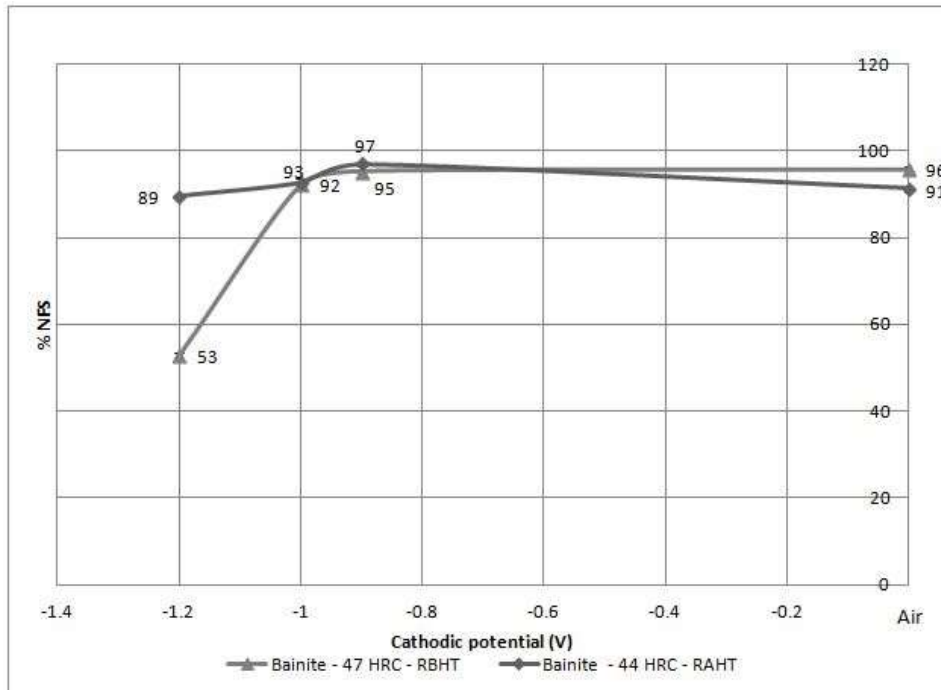


Figure 7.6: Comparison of NFS% drop with increasing cathodic potential for bainite when rolling before and after heat treatment. RAHT showed a less of a NFS% drop.

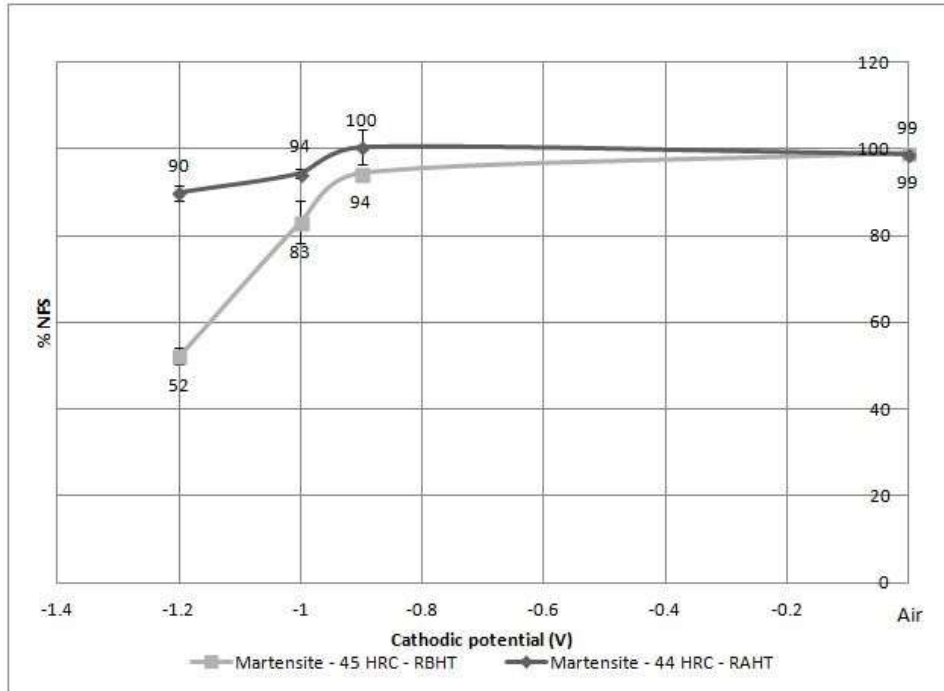


Figure 7.7: Comparison of NFS% drop with increasing cathodic potential for martensite when rolling before and after heat treatment. RAHT showed a less of a NFS% drop.

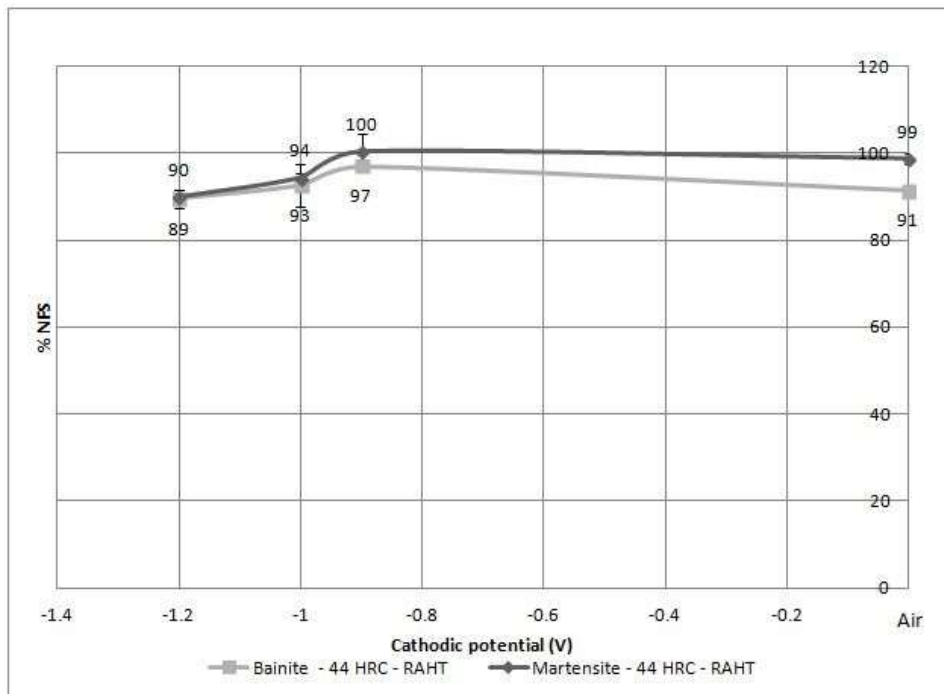


Figure 7.8: Comparison of NFS% drop with increasing cathodic potential for both bainite and martensite when rolling after heat treatment. RAHT showed slight reduction in NFS%.

### 7.5.2 Effect of thread rolling on surface hardness

Figure 7.9 shows the effect of thread rolling on hardness after heat treatment. Thread rolling increased subsurface hardness by approximately 20 %. The increase in hardness is caused by plastic deformation, which results in work hardening owing to an exponential increase in dislocation density. This hardening phenomenon is different from hardening that results from martensite transformation. Figure 7.10 shows the effect of heat treatment after rolling threads (i.e., RBHT). Any hardening effects from cold rolling disappeared once the heat treatment was performed. The hardness is uniform from the surface to the core.

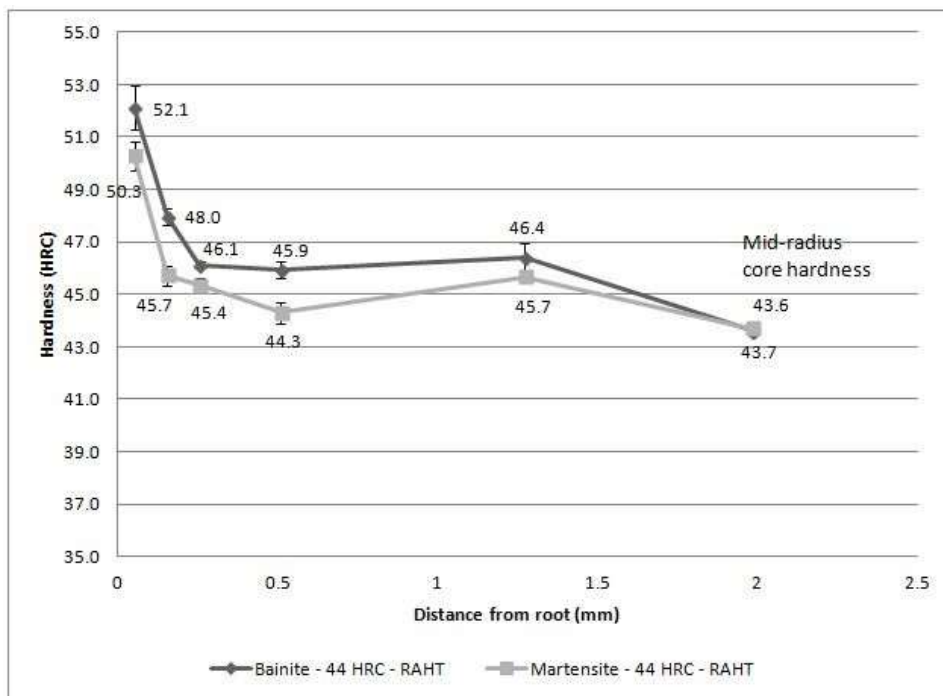


Figure 7.9: Subsurface hardness profile showing the effect of thread rolling after heat treatment – converted from HV0.1.

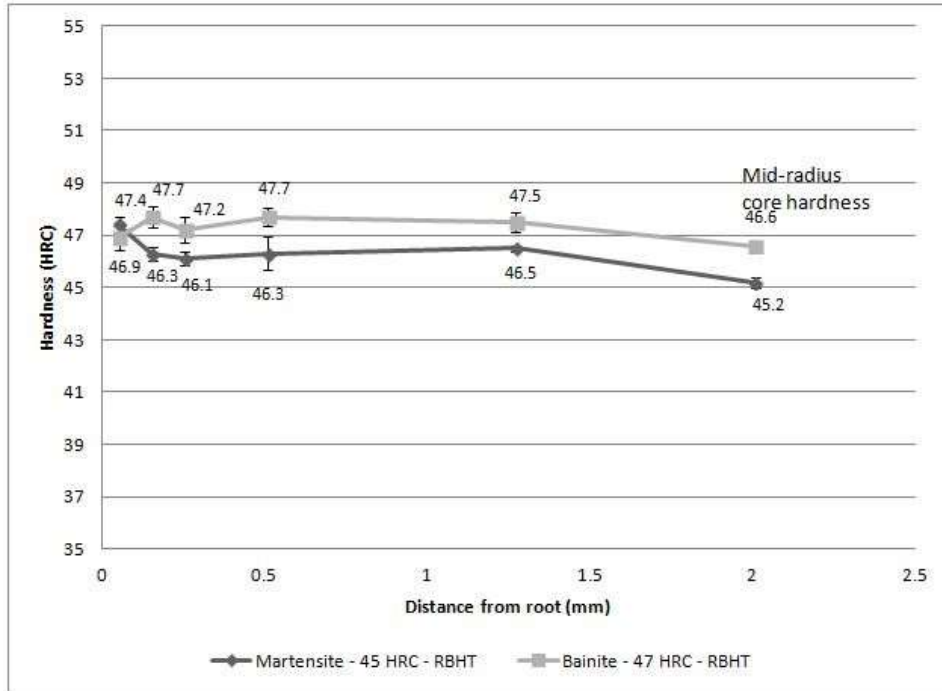


Figure 7.10: Subsurface hardness profile showing the effect of thread rolling before heat treatment – converted from HV0.1.

### 7.5.3 Fracture surface evaluation

Figures 7.11–7.13 show the typical fracture surface zones. Figure 7.11 shows the fracture surface of an FF evaluation. The sample is tested in air under bending stresses at a rapid loading rate of 100 lbs/min. The fractures show a ductile fracture in the initiation zone (Area 1). As the fracture propagates, evidence of a quasi-brittle fracture is observed in Areas 2 and 3. The final (Area 4) still showed evidence of a quasi-brittle fracture.

Figure 7.12 shows the fracture surface of an evaluation performed using a slow step loading rate in air. Again, this will isolate any effect of residual hydrogen that may have been present in the material. The fractures show a ductile fracture in the initiation zone (Area 1). As the fracture propagates, evidence of a quasi-brittle fracture is observed in Areas 2 and 3. The final (Area 4) still showed evidence of a quasi-brittle fracture.

Figure 7.13 shows the fracture surface of an evaluation performed using a slow step loading rate under a  $-1.2$  V cathodic charging condition (tempered martensite). The fracture shows an

intergranular fracture in the initiation zone (Area 1). As the fracture propagates, evidence of a ductile fracture is observed in Areas 2 and 3. The final (Area 4) still showed evidence of a ductile fracture.

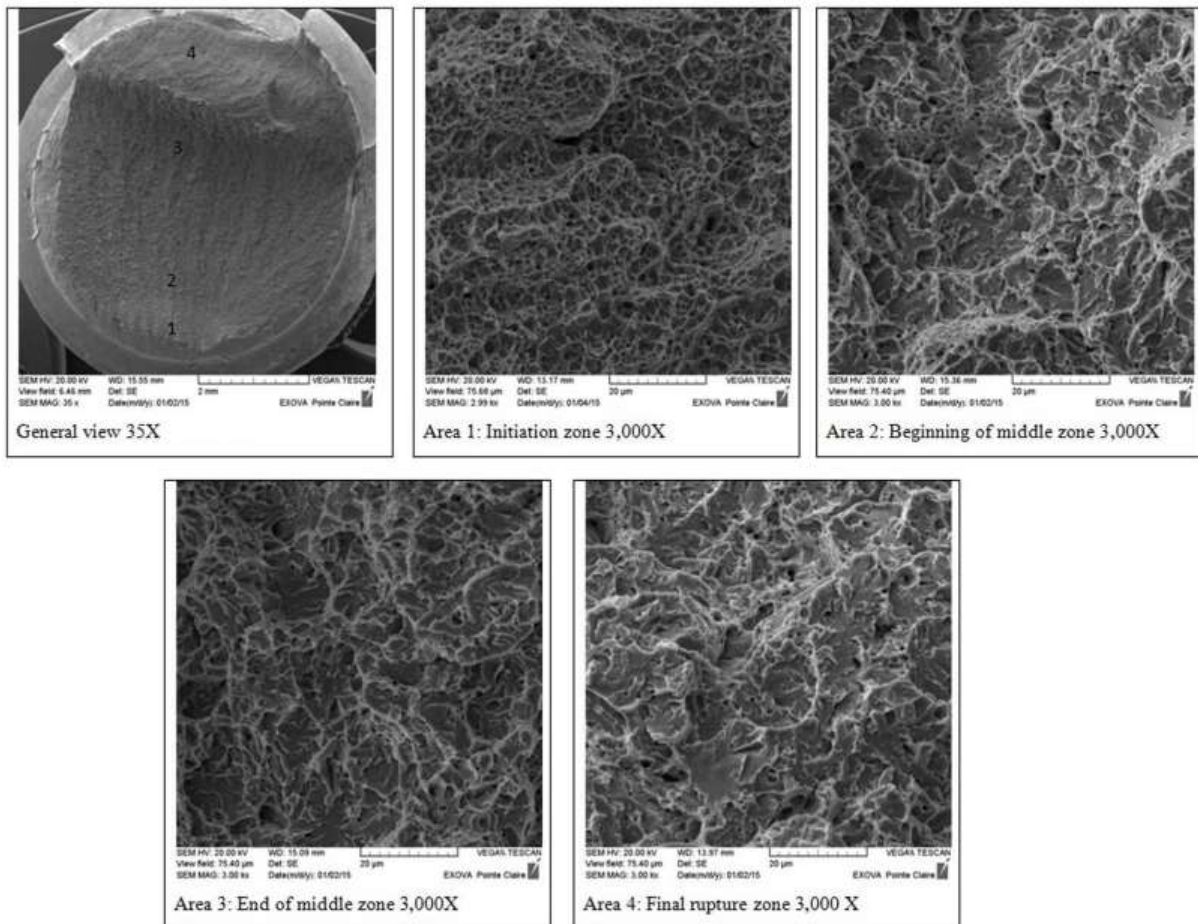


Figure 7.11: Fracture propagation from initiation until final rupture - Lower bainite – RBHT – FF.

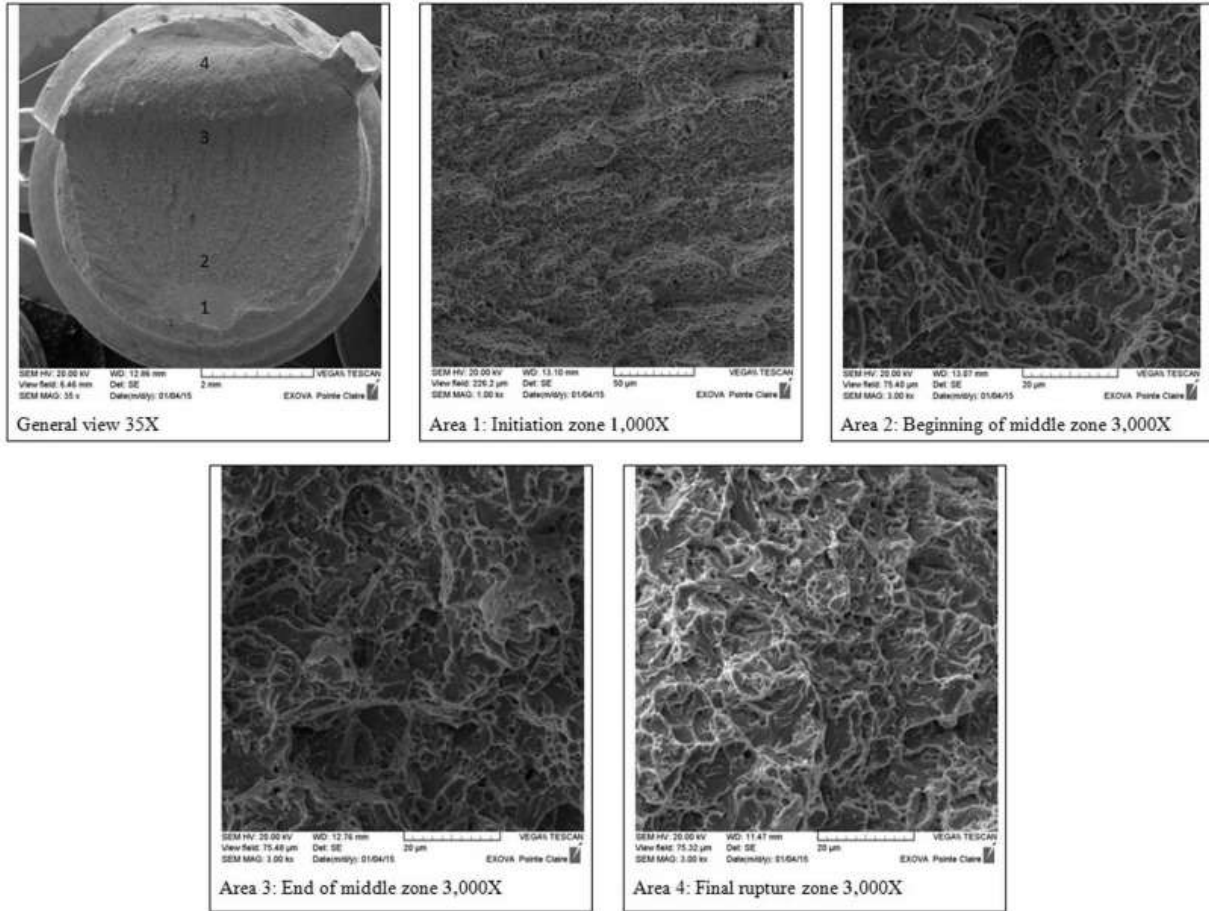


Figure 7.12: Fracture propagation from initiation until final rupture - Lower bainite – RBHT – Air.

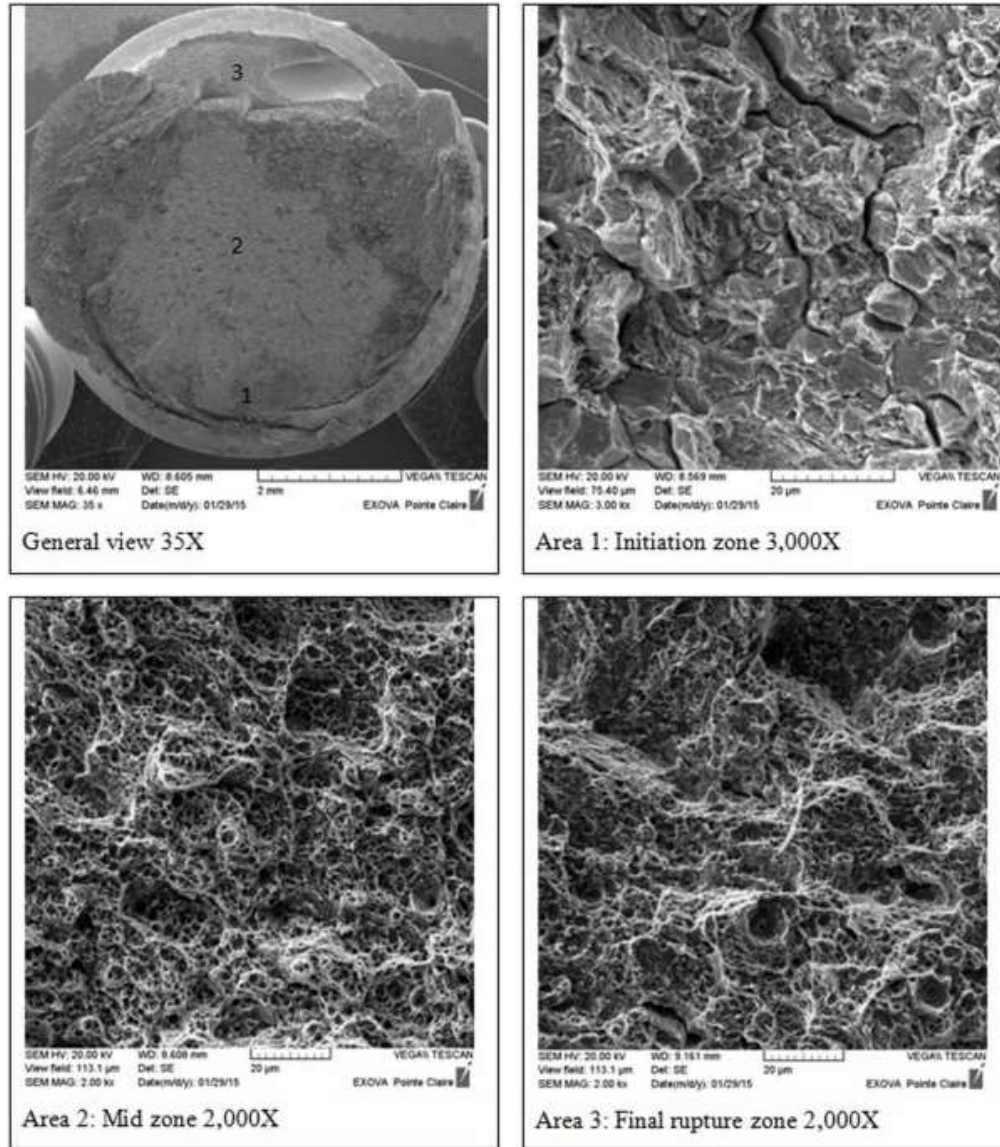


Figure 7.13: Fracture propagation from initiation until final rupture - tempered martensite – RAHT – -1.2V.

## 7.6 Discussion

Previous work, which comprised samples that were rolled before heat treatment, showed bainite had lower susceptibility to HE under moderate hydrogen charging conditions.<sup>6</sup> Results of this current study showed the beneficial effect of rolling after heat treatment for both martensite and bainite microstructures.

Rolling threads is a cold forming process that causes a significant amount of plastic deformation, which in turn results in high localized dislocation density<sup>5</sup> and a localized increase in hardness. These dislocations are eliminated during heat treatment, more precisely during austenitizing.<sup>9,10</sup> When rolling the threads is performed after heat treatment (i.e., as a final processing step) on steel that is hardened, the dislocation density resulting from plastic deformation is exponentially greater than on unhardened steel. Furthermore, these dislocations remain as part of the final material condition. The hardening effect of RAHT is also more pronounced. It should be added, this type of hardening is a different phenomenon from hardening by quenching (i.e., the result of a martensitic transformation). It is important to make this distinction because hardness/strength has been shown to have a first order effect on HE susceptibility. In this case, the opposite effect of hardness on HE susceptibility is observed.

The data show that higher dislocation density correlates with lower HE susceptibility. Dislocations are known hydrogen trap sites<sup>5</sup> that reduce the diffusivity of hydrogen. Consequently, as dislocation density is increased, it follows that less hydrogen is available to participate in the hydrogen damage mechanism. However, in this case the hardening mechanism is different, and therefore the beneficial outcome of rolling after heat treatment does not contradict the established correlation between transformation hardness and HE susceptibility.

Finally, whereas it was previously shown that bainite results in marginal reduction of HE susceptibility under moderate hydrogen charging conditions (i.e.,  $-1.0$  V), this work showed no measurable difference between martensite and bainite with RAHT. Dislocations introduced by cold rolled threads evidently override any effect of microstructure on hydrogen transport and trapping and therefore on HE susceptibility.

## **7.7 Conclusion**

The objective of this study was to investigate the effects of microstructure on the susceptibility of steel fasteners to HE. More precisely, the study compares quenched and tempered martensite and lower bainite obtained by austempering in both of the following conditions: RBHT and RAHT.

At the most severe H charging condition of  $-1.2$  V, NFS% results were found significantly improved in the RAHT condition compared to RBHT, independent of the microstructure. RAHT

resulted in no discernible ductile to brittle transition with increasing hydrogen charging. The ductile to brittle transition was evident for RBHT samples.

Results showed the beneficial effect of rolling after heat treatment for both martensite and bainite microstructures. The data show that higher dislocation density correlates with lower HE susceptibility.

## 7.8 References

1. L. Raymond, "Evaluation of Hydrogen Embrittlement," in *ASM Metals Handbook*, Vol. 13 (Materials Park, OH: ASM International, 1987), 283–290.
2. B. Craig, "Hydrogen Damage," in *ASM Metals Handbook*, Vol. 13 (Materials Park, OH: ASM International, 1987), 163–171.
3. S. V. Brahim, S. Yue, and K. R. Sriraman, "Alloy and Composition Dependence of Hydrogen Embrittlement Susceptibility in High Strength Steel Fasteners," *Philosophical Transactions of the Royal Society A* 375, no. 2098 (2017): 20160407, <https://doi.org/10.1098/rsta.2016.0407>
4. R. Cioto and A. Collares, *Reduction of Fatigue Resistance on Bolts with Threads Rolled after Heat Treatment, as a Result of Superficial Treatment*, SAE Technical Paper 2003-01-3657 (Warrendale, PA: SAE International, 2003), <https://doi.org/10.4271/2003-01-3657>
5. N. Horn and R. Stephens, "Influence of Cold Rolling Threads before or after Heat Treatment on High Strength Bolts for Different Fatigue Preload Conditions," *Journal of ASTM International* 3, no. 1 (January 2006): 1–21, <https://doi.org/10.1520/JAI12551>
6. F. Saliby, S. Brahim, S. Rajagopalan, and S. Yue, "Hydrogen Embrittlement Susceptibility of Bainite for High Strength Steel Fasteners," *Materials Performance and Characterization* 6, no. 1 (November 2017): 462–471, <https://doi.org/10.1520/MPC20170060>

7. *Standard Test Method for Measurement of Hydrogen Embrittlement Threshold in Steel by the Incremental Step Loading Technique* (Superseded), ASTM F1624-12 (West Conshohocken, PA: ASTM International, approved August 1, 2012), <https://doi.org/10.1520/F1624-12>
8. *Standard Test Method for Process Control Verification to Prevent Hydrogen Embrittlement in Plated or Coated Fasteners* (Superseded), ASTM F1940-07a(2014) (West Conshohocken, PA: ASTM International, approved September 1, 2007), <https://doi.org/10.1520/F1940-07AR14>
9. M. Blair and T. L. Stevens, *Steel Castings Handbook*, 6th ed. (Materials Park, OH: ASM International, 1995).
10. M. Pfeifer, *Materials Enabled Designs: The Materials Engineering Perspective to Product Design and Manufacturing* (Oxford, UK: Butterworth-Heinemann, 2009).

## Chapter 8 : Discussion

The objective of this study was to evaluate the role of microstructure on HE susceptibility of high strength steel fasteners; more specifically, to compare the HE susceptibility of tempered martensite to lower bainite. In addition, the effect of thread rolling performed after heat treatment on HE susceptibility was evaluated.

### 8.1 Effect of lower bainite microstructure

Results show that at equivalent hardness (i.e., 45 HRC) and under moderate hydrogen charging condition (i.e., -1.0 V), lower bainite exhibited marginally higher threshold stress, i.e., lower HE susceptibility. Two hypotheses are proposed to explain the slight reduction in susceptibility.

The first hypothesis considers the bulk mechanical properties of lower bainite. It is generally accepted and furthermore demonstrated in this research, that lower bainite exhibits slightly greater ductility than tempered martensite [39]. More ductility correlates with a higher rate of dislocation emission and plastic deformation. It follows that lower bainite, being more ductile than tempered martensite at equal strength, is naturally slightly less prone to cracking. With the addition of hydrogen, lower bainite's higher propensity for dislocation emission when compared to tempered martensite under equal strength and hydrogen charging conditions is apparently maintained. Song and Curtin proposed that the nature of hydrogen interaction is to promote dislocation pinning [40]. Given equal quantity of hydrogen in each material, even a slightly higher rate of emission dislocation in lower bainite can lessen the effect of hydrogen interaction and delay grain boundary decohesion, effectively lowering HE susceptibility.

The second hypothesis considers hydrogen transportation and trapping behaviors. Although martensite and bainite are very similar structures, small differences in microstructural features that are hydrogen traps, e.g., precipitates, grain boundaries, dislocations, etc., can hypothetically result in different rates of hydrogen transport and trapping. In other words, lower bainite may be less embrittled because the microstructure has a higher capacity to trap hydrogen [41].

For example, although Bhadeshia measured similar dislocation densities between bainite and tempered martensite (i.e.,  $10^{15} \text{ m}^{-2}$ ), he also found that average cementite can be approximately six times smaller in tempered martensite than in lower bainite (38 nm vs. 230 nm) while having

approximately same overall volume fraction [42]. The coarser cementite precipitates in bainite may conceivably result in a marginally greater propensity for irreversible trapping, and a plausible contributor to slightly lower HE susceptibility of lower bainite.

The question of hydrogen transportation and trapping behavior may be investigated in future work aimed at characterizing hydrogen trapping capacity in both materials by means of electrochemical permeation and thermal desorption experiments.

## **8.2 Effect of rolling threads after heat treatment**

Results showed the beneficial effect of rolling threads after heat treatment for both tempered martensite and lower bainite microstructures. Thread rolling is a cold forming process that causes significant amount of plastic deformation, which in turn results in high localized dislocation density [32] and localized increase in hardness. These dislocations are eliminated during heat treatment, more precisely during austenitizing [43] [44]. When thread rolling is performed after heat treatment (i.e., as a final processing step) on steel that is hardened, the dislocation density resulting from plastic deformation is exponentially greater than on unhardened steel.

The results show that higher dislocation density correlates with lower HE susceptibility. Dislocations are known hydrogen trap sites [32] that reduce the diffusivity of hydrogen. Consequently, as dislocation density is increased it follows that less hydrogen is available to participate in the hydrogen damage mechanism. These dislocations remain as part of the final material condition. The hardening effect of rolling of threads after heat treatment is also more pronounced. It should be reminded that typical hardness/strength increase (from heat treatment) has been shown to have a first order effect on HE susceptibility [45]. In this case, the hardness/strength increase (from plastic deformation) reduces HE susceptibility. This demonstrates that plastic deformation has an even greater effect on HE susceptibility than hardness from heat treatment. Both these hardening mechanisms are different, and therefore the beneficial outcome of rolling after heat treatment does not contradict the established correlation between transformation hardness and HE susceptibility.

Another aspect to consider is that the application of compressive stress counteracts the tensile forces, effectively reducing tensile stresses. This reduction of tensile stress has been shown to be beneficial for increasing fatigue life. In the context of HE, it appears to also contribute to increasing

HE resistance of the fastener. The current experimental conditions do not isolate the effect of compressive stress versus the effect of dislocations, principally because the two factors are codependent. Therefore, it is not possible to determine which of the two play a more significant role.

Finally, lower bainite results had marginal HE susceptibility improvements under moderate hydrogen charging conditions (i.e., -1.0 V). However, when threads are rolled after heat treatment (i.e., higher dislocation density), both lower bainite and tempered martensite had no measurable HE susceptibility difference. The combined effect of dislocations and compressive stress introduced by cold rolling after heat treatment evidently overrides any effect of microstructure on hydrogen transportation and trapping, and therefore on HE susceptibility.

Based on the correlation between plastic deformation and lower HE susceptibility, thread rolling after heat treatment should be adopted as a standard requirement for ultra high strength fasteners.

Future work needs to evaluate the effect of rolling threads after heat treatment on different thread characteristics (i.e., thread types and sizes).

## Chapter 9 : Conclusions

The first objective of this research was to compare the effects of microstructures of quenched and tempered martensite and lower bainite obtained by austempering on the susceptibility of steel fasteners to hydrogen embrittlement. The second objective was to investigate the effect on HE susceptibility of rolling threads before and after heat treatment.

The following conclusions were derived from this study:

1. In the rolled before heat treatment condition, lower bainite exhibited marginally higher notch fracture strength at moderate charging condition (-1.0 V).
2. In the rolled after heat treatment condition, notch fracture strength was significantly higher compared to rolled before heat treatment, independent of the microstructure or the core hardness.
3. Rolled after heat treatment resulted in no discernible ductile to brittle transition with increasing hydrogen charging. The ductile to brittle transition was evident for threads rolled before heat treatment samples.
4. Results showed the beneficial effect of rolling threads after heat treatment for both martensite and bainite microstructures, leading to the hypothesis that the combined effect higher dislocation density and compressive stress correlates with lower hydrogen embrittlement susceptibility.

In conclusion, despite the finding that lower bainite has marginally lower HE susceptibility when compared to tempered martensite, given that strength has a first order affect on HE susceptibility, it remains that at strength levels above 1200 MPa, both structures are highly susceptible to HE. Therefore, the use of bainitic ultrahigh strength fasteners is not justified based on HE susceptibility. Given that ductility and toughness are desirable material properties for high strength fasteners used in critical applications, the use of bainitic ultrahigh strength fasteners is better justified considering the ability of bainite to retain a greater degree of ductility and toughness at those high strength levels.

## **Chapter 10 : Future work**

Future work is recommended along two tracks to validate the hypotheses drawn from this study, notably on the effects of microstructure (i.e., bainite vs. martensite), and dislocation density on hydrogen embrittlement susceptibility. It may also be revealing to explore and design novel experiments that aim to isolate the effects of dislocation density versus compressive stress, for example by creating dislocations under tensile stress.

### **10.1 Effect of microstructure – bainite vs. martensite**

Lower bainite and tempered martensite are very similar, and even indistinguishable, thus requiring tedious examination to observe differences. At high magnification, differences have been reported in the nature of precipitates (i.e. carbides) that can affect hydrogen transport and trapping, as a result of differences in shape, size, compositions, and distribution. Carbide arrangement is observed under a transmission electron microscope (TEM). A close examination of these differences, combined with characterization of trap sites and diffusivity by means of electrochemical permeation (EP) experiments and thermal desorption spectroscopy (TDS) may reveal the cause of the slightly lower susceptibility of bainite.

### **10.2 Effect of plastic deformation and dislocation density**

Rolling threads after heat treatment showed significantly lower HE susceptibility in both microstructures. It was hypothesized that the resulting high localized dislocation density helped increase hydrogen trapping, which in turn marginally increased the HE threshold for bainite. Here, isolating the effect of dislocation-based trapping and resulting hydrogen diffusivity by means of electrochemical permeation (EP) experiments and thermal desorption spectroscopy (TDS) could confirm the validity of the hypothesis. In such a study, the degree of plastic deformation and the resulting dislocation densities should be considered as a variable. This is relevant for fasteners because plastic deformation varies as a function of different thread characteristics (e.g., thread type and size).

## References

Note: This reference section pertains to all sections except Chapters 6 and 7.

1. *Hydrogen Damage and Embrittlement*, in *Failure Analysis and Prevention*, W.T. Becker and R.J. Shipley, Editors. 2002, ASM International. p. 0.
2. *Corrosion: Fundamentals, Testing, and Protection*, ed. S.D. Cramer and B.S. Covino, Jr. 2003: ASM International.
3. Committee, A.H., *Properties and Selection: Irons, Steels, and High-Performance Alloys*. 1990: ASM International.
4. Colpaert, H. and A.L.V. da Costa e Silva, *Metallography of Steels: Interpretation of Structure and the Effects of Processing*. 2018: ASM International.
5. *Surface Engineering*, ed. C.M. Cotell, J.A. Sprague, and F.A. Smidt, Jr. 1994: ASM International.
6. Oriani, R.A., *The Physical and Metallurgical Aspects of Hydrogen in Metals*. ICCF4, 1993.
7. *ASTM F2075-15, Standard Terminology Relating to Hydrogen Embrittlement Testing*, in *ASTM International*. 2015: West Conshohocken, PA.
8. Nagao, A., et al., *The role of hydrogen in hydrogen embrittlement fracture of lath martensitic steel*. Acta Materialia, 2012. **60**(13-14): p. 5182-5189.
9. Zapffe, C.A.S., C.E., *Hydrogen Embrittlement, Internal Stress. and Defects in Steel*. . Am. Inst. Mining Met Engrs. Tech. Pub., 1941. **1307**: p. 1-37.
10. Birnbaum, H.K. and P. Sofronis, *Hydrogen-enhanced localized plasticity -a mechanism for hydrogen related fracture* Materials Science and Engineering a-Structural Materials Properties Microstructure and Processing, 1994. **176**(1-2): p. 191-202.
11. Hwang, C.B., I.M., *Dislocation transport of hydrogen in iron single crystals*. Acta Metallurgica, 1985. **34**(6): p. 1001-1010.
12. Tien, J., et al., *Hydrogen transport by dislocations*. Metallurgical Transactions A, 1976. **7**(6): p. 821-829.
13. Pressouyre, G.M., *Trap theory of Hydrogen embrittlement*. Acta Metallurgica, 1980. **28**(7): p. 895-911.
14. Krom, A.H.M., Bakker A., *Hydrogen Trapping Models in Steel*. Metallurgical and Materials Transactions A: Physical Metallurgy and Materials Science, 2000. **31B**(December): p. 1475-1482.
15. Grabke H. J., R., *Absorption and diffusion of hydrogen in steels*. MATERIALI IN TEHNOLOGIJE, 2000(34): p. 331-342.
16. Lупpo, M.I. and J. Ovejero-Garcia, *The influence of microstructure on the trapping and diffusion of hydrogen in a low carbon steel*. Corrosion Science, 1991. **32**(10): p. 1125-1136.

17. Brahim, S., *Effect of Surface Processing Variables on Hydrogen Embrittlement of Steel Fasteners*. 2007: McGill University Libraries.
18. *ASTM F1941-16, Standard Specification for Electrodeposited Coatings on Mechanical Fasteners, Inch and Metric*, in *ASTM International*. 2016: West Conshohocken, PA.
19. *USCAR – IFI GUIDE for Ultra-high Strength Externally Threaded Fasteners*. 2015.
20. *Heat Treating*. Vol. 4. 1991: ASM International.
21. Wright, W.W., *Materials science and engineering. An introduction 2nd Edition W. D. Callister, Jr John Wiley & Sons, New York, 1991. pp. xxi + 791, price E53.00. ISBN 0-471-50488-2*. Polymer International, 1993. **30**(2): p. 282-283.
22. Bhadeshia, H.K.D.H. and H.K.D.H. Bhadeshia, *Bainite in Steels: Transformations, Microstructure and Properties*. 2001: IOM Communications.
23. Troiano, A.R., Heheman R. F., *Hydrogen embrittlement and stress corrosion cracking in sour environment*. 1982. **ASM**(Current solutions to hydrogen embrittlement problems in steels): p. 299-307.
24. *ASTM E8 / E8M-16, Standard Test Methods for Tension Testing of Metallic Materials*, in *ASTM International*. 2016: West Conshohocken, PA.
25. Pollock, W.J., *Assessment of the Degree of Hydrogen Embrittlement Produced in High-Strength 4340 Steel by Plating-and-Baking Processes Using Slow Strain Rate Testing*, L. Raymond, Editor. 1988, ASTM International: West Conshohocken, PA. p. 68-85.
26. *ISO 7539-7:2005, Corrosion of metals and alloys — Stress corrosion testing — Part 7: Method for slow strain rate testing*. 2005.
27. *ASTM G129-00(2013), Standard Practice for Slow Strain Rate Testing to Evaluate the Susceptibility of Metallic Materials to Environmentally Assisted Cracking*, in *ASTM International*. 2013: West Conshohocken, PA.
28. *ASTM F1624-12, Standard Test Method for Measurement of Hydrogen Embrittlement Threshold in Steel by the Incremental Step Loading Technique*, in *ASTM International*. 2012: West Conshohocken, PA.
29. *ISO 7539-6, Corrosion of metals and alloys — Stress corrosion testing — Part 6: Preparation and use of precracked specimens for tests under constant load or constant displacement*. 2003.
30. *ASTM F1940-07a, Standard Test Method for Process Control Verification to Prevent Hydrogen Embrittlement in Plated or Coated Fasteners*, in *ASTM International*. 2007: West Conshohocken, PA.
31. Cioto, R. and A.R. Collares, *Reduction of Fatigue Resistance on Bolts with Threads Rolled after Heat Treatment, as a Result of Superficial Treatment*. 2003, SAE International.
32. Horn, N. and R. Stephens, *Influence of Cold Rolling Threads Before or After Heat Treatment on High Strength Bolts for Different Fatigue Preload Conditions*. Journal of Astm International, 2006. **3**: p. 1-21.

33. *ASTM E18-15, Standard Test Methods for Rockwell Hardness of Metallic Materials*, in *ASTM International*. 2016: West Conshohocken, PA.
34. *ASTM F606 / F606M-14a, Standard Test Methods for Determining the Mechanical Properties of Externally and Internally Threaded Fasteners, Washers, Direct Tension Indicators, and Rivets*, in *ASTM International*. 2016: West Conshohocken, PA.
35. *ASTM E384-11e1, Standard Test Method for Knoop and Vickers Hardness of Materials*, in *ASTM International*. 2016: West Conshohocken, PA.
36. Saliby, F., Brahimy, S., Rajagopalan, S., and Yue, S., *Hydrogen Embrittlement Susceptibility of Bainite for High Strength Steel Fasteners*. *Materials Performance and Characterization*, 2017. **6**(1): p. 462-471.
37. Saliby, F., Brahimy, S., Rajagopalan, S., and Yue, S., *Effect of Rolling after Heat Treatment on Hydrogen Embrittlement Susceptibility for High Strength Steel Fasteners*. *Materials Performance and Characterization*, 2020. **9**(1): p. 549-560.
38. *ASTM E3-11, Standard Guide for Preparation of Metallographic Specimens*, in *ASTM International*. 2011: West Conshohocken, PA.
39. Totten, G.E., *Steel Heat Treatment Handbook, Second Edition - 2 Volume Set*. 2006: Taylor & Francis.
40. Song, J. and W.A. Curtin, *Atomic mechanism and prediction of hydrogen embrittlement in iron*. *Nature Materials*, 2013. **12**(2): p. 145-151.
41. Fleurentin, A., Creus, J., and Feaugas, X., *Impact de la Structure Métallurgique sur le Chargement et la Désorption Naturelle de L'Hydrogène dans un acier (37Cr4) Traite à 1250 MPa*. Cetim, 2013.
42. Bhadeshia, H., *Martensite and Bainite in Steels : Transformation Mechanism & Mechanical Properties*. *Journal de Physique IV Proceedings*, 1997. **07**(C5): p. C5-367-C5-376.
43. Blair, M. and T.L. Stevens, *Steel Castings Handbook, 6th Edition*. 1995: Steel Founders' Society of America.
44. Pfeifer, M., *Materials Enabled Designs: The Materials Engineering Perspective to Product Design and Manufacturing*. 2009: Elsevier Science.
45. Brahimy S. V., Y.S.a.S.K.R., *Alloy and composition dependence of hydrogen embrittlement susceptibility in high-strength steel fasteners*. *The Royal Society Publishing*, 2017. **375**(2098).

## **Appendix 1: Complementary results**

The following section describes methodologies and findings during microstructural and fractographic evaluations that were excluded from the two manuscripts.

### **A1.1 Microstructure**

Microstructural evaluations were performed using standard sectioning, mounting and polishing techniques per ASTM E3 [38]. Samples were wet ground with 120, 240, 320, 400, 600 and 800 grit SiC paper followed by polishing with 3  $\mu\text{m}$  and 1  $\mu\text{m}$  diamond suspension. Final polishing with 0.5 $\mu\text{m}$  alumina solution was performed to obtain a mirror finish. The microstructure was revealed by etching with 2% nital (2 ml of nitric acid ( $\text{HNO}_3$ ) in 98 ml of ethanol) for tempered martensite and lower bainite. Also, 10% sodium metabisulfite (10 g of sodium metabisulfate ( $\text{Na}_2\text{S}_2\text{O}_5$ ) in 90 ml of water) was also used for lower bainite.

Evaluation was performed using an Olympus PMG3 light microscope with magnification capabilities from 40 to 800 X. Figure A 1 and Figure A 3 show the microstructure of tempered martensite of samples B3 (45 HRC / RBHT) and B9 (44 HRC / RAHT) respectively. The structures consist of finely distributed carbides with lath martensite. Figure A 2 and Figure A1 4 show the microstructure of lower bainite of samples B4 (47 HRC / RBHT) and B8 (44 HRC / RAHT) respectively. Differencing between both microstructures was not possible under optical nor scanning electron microscopy (SEM). Using a transmission electron microscopy (TEM) with higher magnification capabilities would have been required to differentiate the aligned carbides of lower bainite.

Kamax Automotive GmbH also performed microstructural evaluations and confirmed the presence of both microstructures, i.e., tempered martensite and lower bainite.

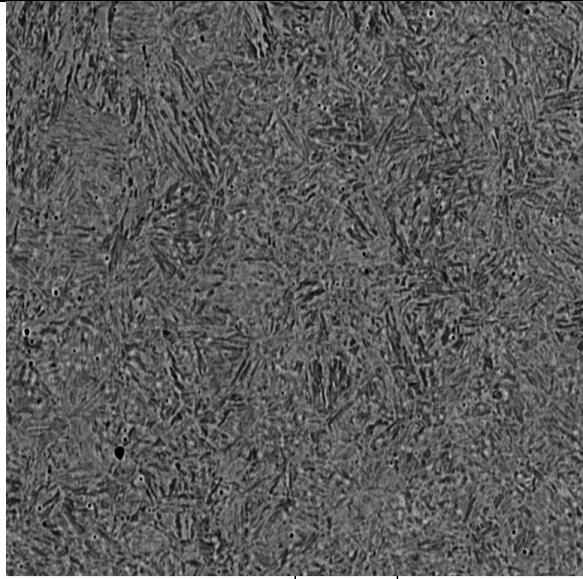
	
<p>Optical / Magnification 500X / Nital 2% etch (Source : Kamax Automotive GmbH)</p>	<p>SEM / Magnification 2000X / Nital 2% etch</p>

Figure A 1: B3 – Optical and SEM images showing a tempered martensite microstructure (RBHT).

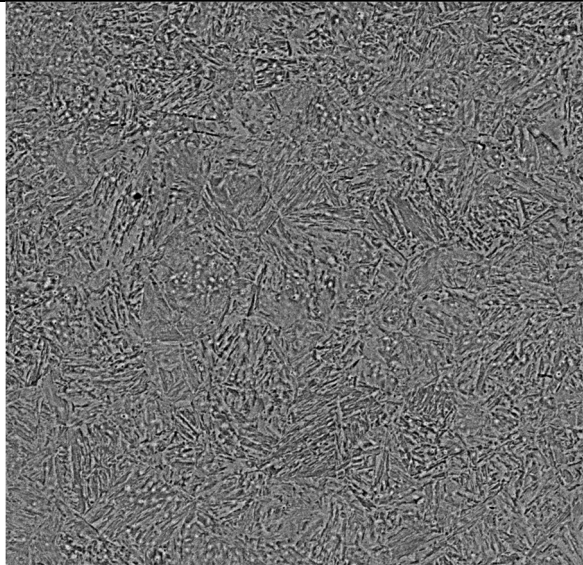
	
<p>Optical / Magnification 500X / Nital 2% etch (Source : Kamax Automotive GmbH)</p>	<p>SEM / Magnification 2000X / Nital 2% etch</p>

Figure A 2: B4 – Optical and SEM images showing a lower bainite microstructure (RBHT).

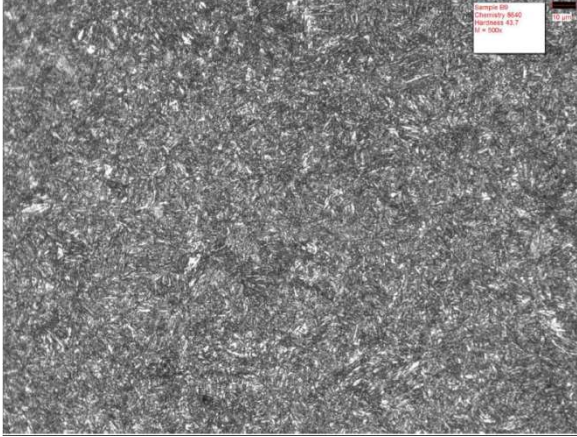
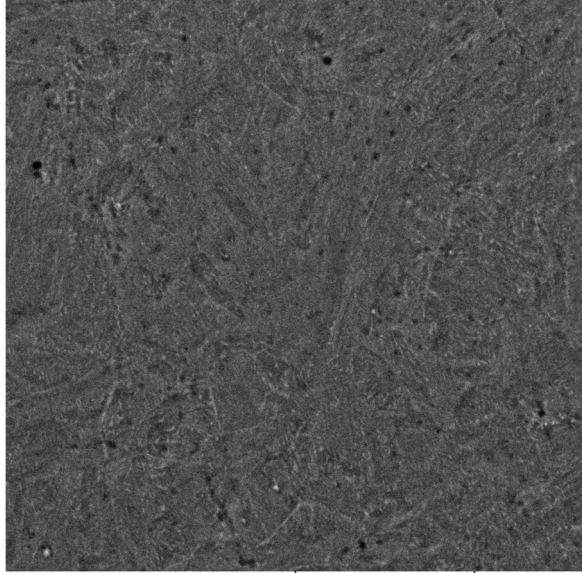
	 <p>SEM HV: 20.00 kV    WD: 8.044 mm    VEGA\\ TESCAN View field: 32.31 μm    Det: SE SEM MAG: 7.00 kx    Date(m/d/y): 07/22/15    10 μm    EXOVA Pointe Claire</p>
<p>Optical / Magnification 500X / Nital 2% etch (Source Kamax Automotive GmbH)</p>	<p>SEM / Magnification 7000X / 10% sodium metabisulfite etch</p>

Figure A 3: B9 – Optical and SEM images showing a tempered martensite microstructure (RAHT – high hardness).

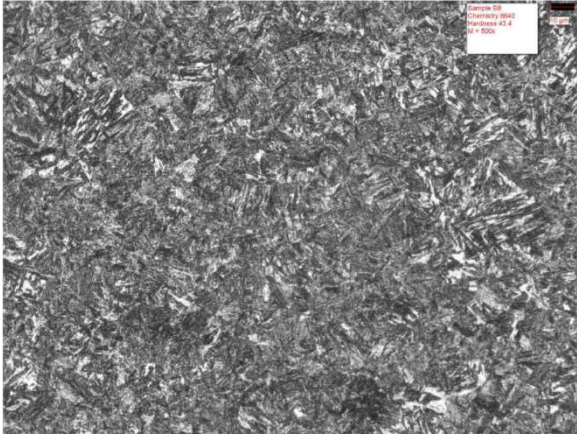
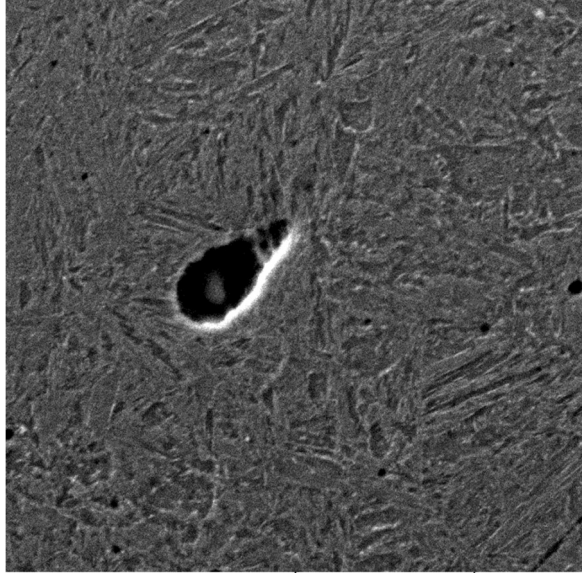
	 <p>SEM HV: 20.00 kV    WD: 7.780 mm    VEGA\\ TESCAN View field: 32.31 μm    Det: SE SEM MAG: 7.00 kx    Date(m/d/y): 07/22/15    10 μm    EXOVA Pointe Claire</p>
<p>Optical / Magnification 500X / Nital 2% etch (Source Kamax Automotive GmbH)</p>	<p>SEM / Magnification 7000X / 10% sodium metabisulfite etch</p>

Figure A 4: B8 – Optical and SEM images showing a lower bainite microstructure (RAHT – high hardness).

## **A1.2 Fractography**

Fractography was evaluated with a Tescan Vega scanning electron microscope (SEM). Figure A 5 to A 10 show the fracture propagation at a -1.0 V hydrogen charging condition.

### **A1.2.1 Fracture surface – -1.0 V Hydrogen Charging Condition – Rolled before HT – 45 HRC**

Figure A 5 shows the general view of the fracture surface of the lower bainite sample. The fracture shows a quasi-brittle fracture from the initiation zone up until the final fracture zone which is fully ductile. Figure A 6 shows the general view of the fracture surface of the tempered martensite sample. The fracture shows an intergranular fracture in the initiation zone and transitions to a ductile fracture until the final fracture zone.

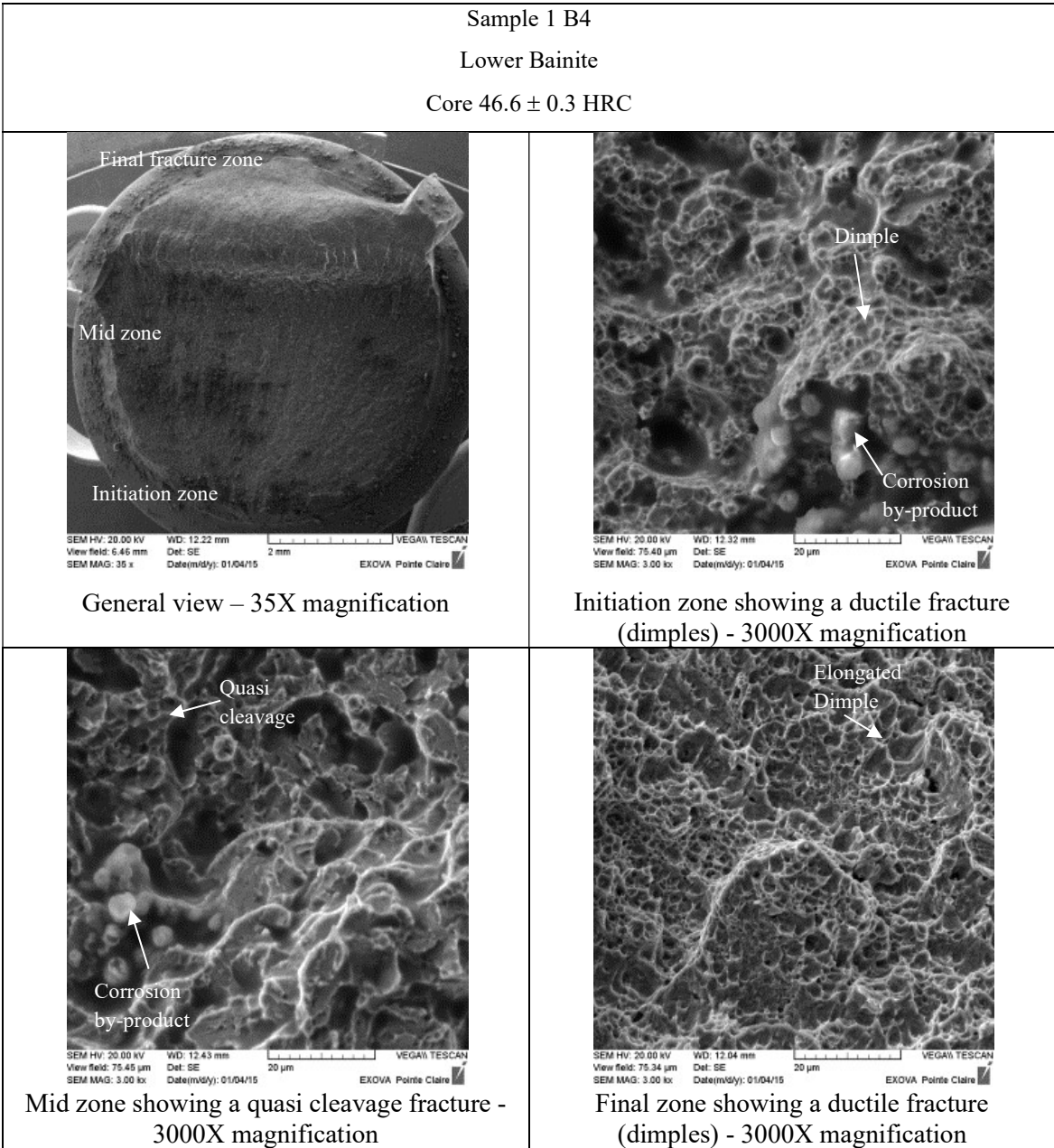


Figure A 5: Fracture surface progression during ISL evaluation of lower bainite at -1.0 V hydrogen charging condition (RBHT).

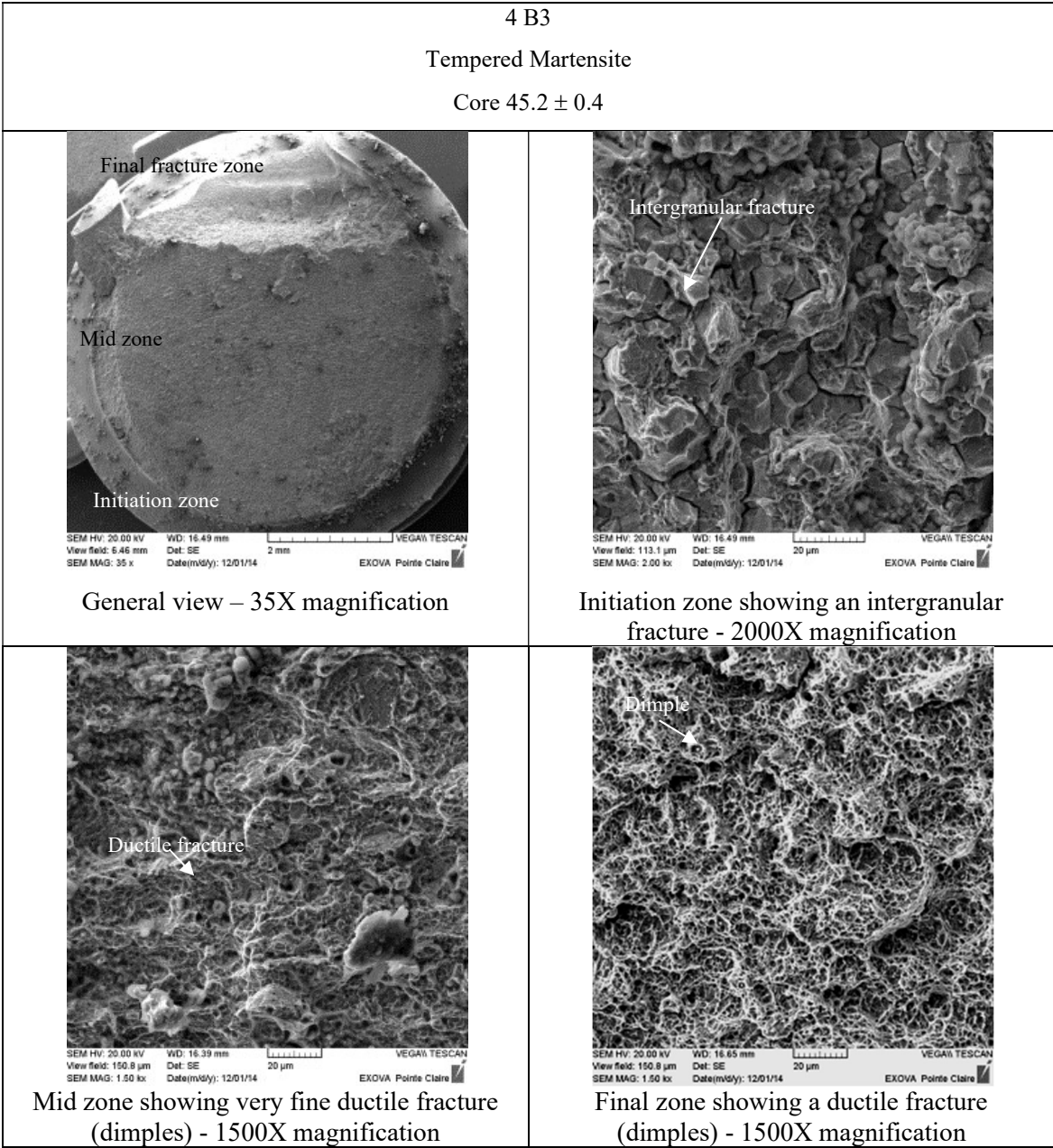


Figure A 6: Fracture surface progression during ISL evaluation of tempered martensite at -1.0 V hydrogen charging condition (RBHT).

### A1.2.2 Fracture surface – -1.0 V Hydrogen Charging Condition – Rolled after HT – 39 HRC

Figure A 7 shows the general view of the fracture surface of the lower bainite sample. The initiation zone fracture is transgranular (i.e., brittle). The crack propagation is transgranular until the final fracture zone which is fully ductile. Figure A 8 shows the general view of the fracture

surface of the tempered martensite sample. The fracture surface was too corroded in the initiation zone. Away from the initiation zone, a ductile fracture is visible until the final fracture zone.

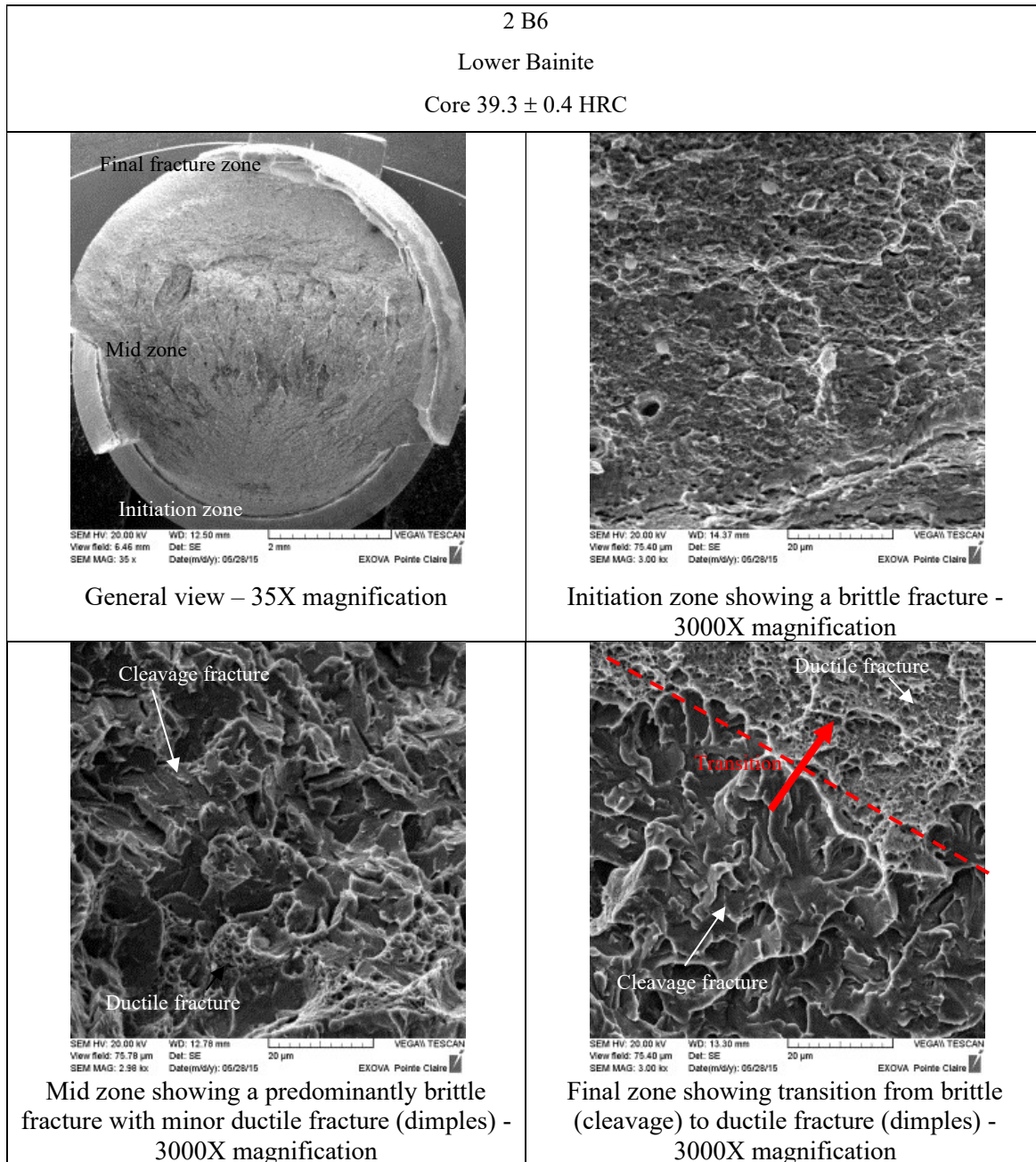


Figure A 7: Fracture surface progression during ISL evaluation of lower bainite at -1.0 V hydrogen charging condition (RAHT / Low hardness).

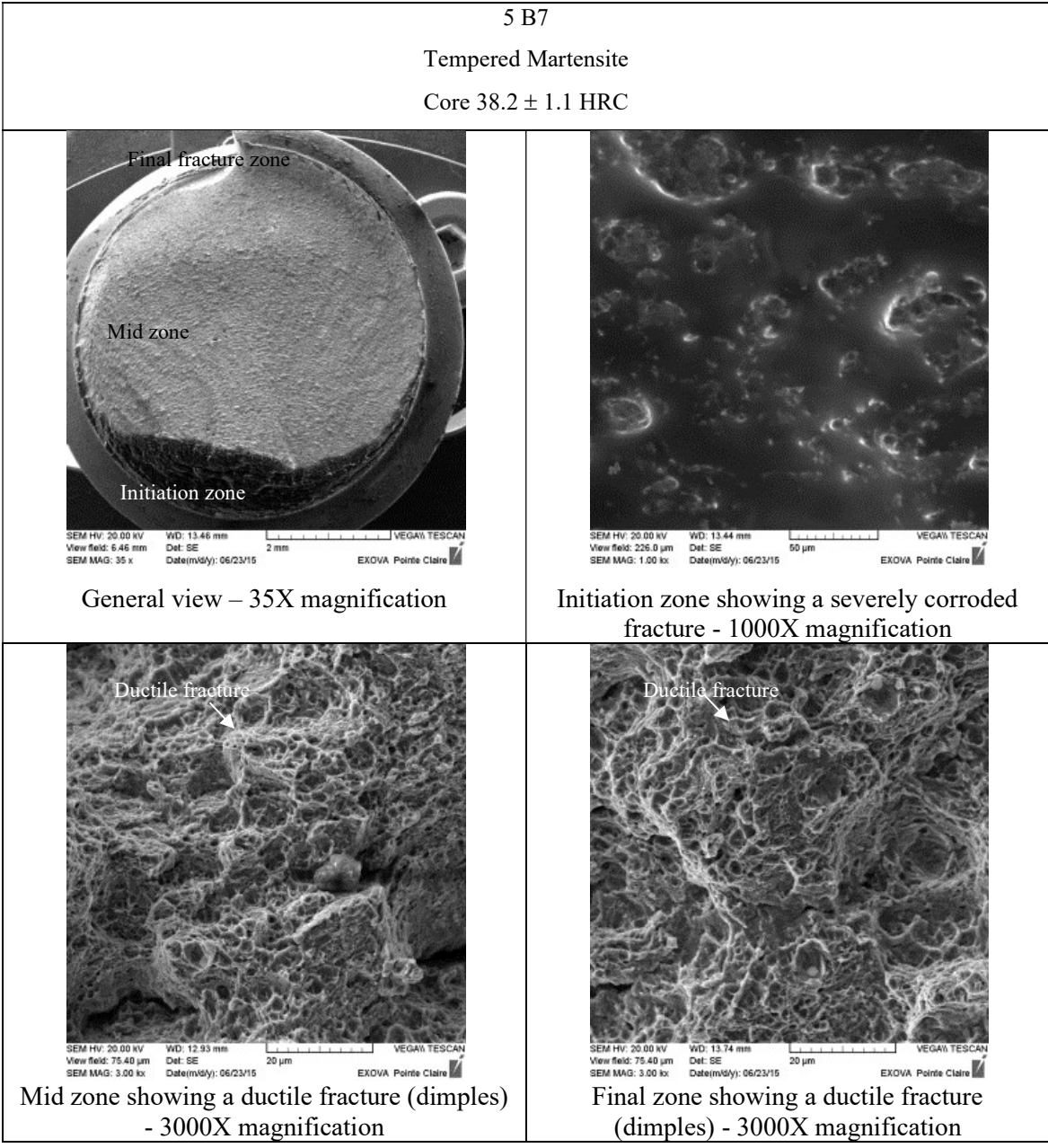


Figure A 8: Fracture surface progression during ISL evaluation of tempered martensite at -1.0 V hydrogen charging condition (RAHT / Low hardness).

**A1.2.3 Fracture surface – -1.0 V H Charging Condition – Rolled after HT – 45 HRC**

Figure A 9 shows the general view of the fracture surface of the lower bainite sample. In fact, it consists of a very fine ductile fracture in the initiation zone. Further from the initiation zone, the fracture becomes quasi brittle until the final fracture zone which is fully brittle. Figure A 10 shows

the general view of the fracture surface of the tempered martensite sample. The fracture shows an intergranular fracture in the initiation zone and transitions to a ductile fracture until the final fracture zone.

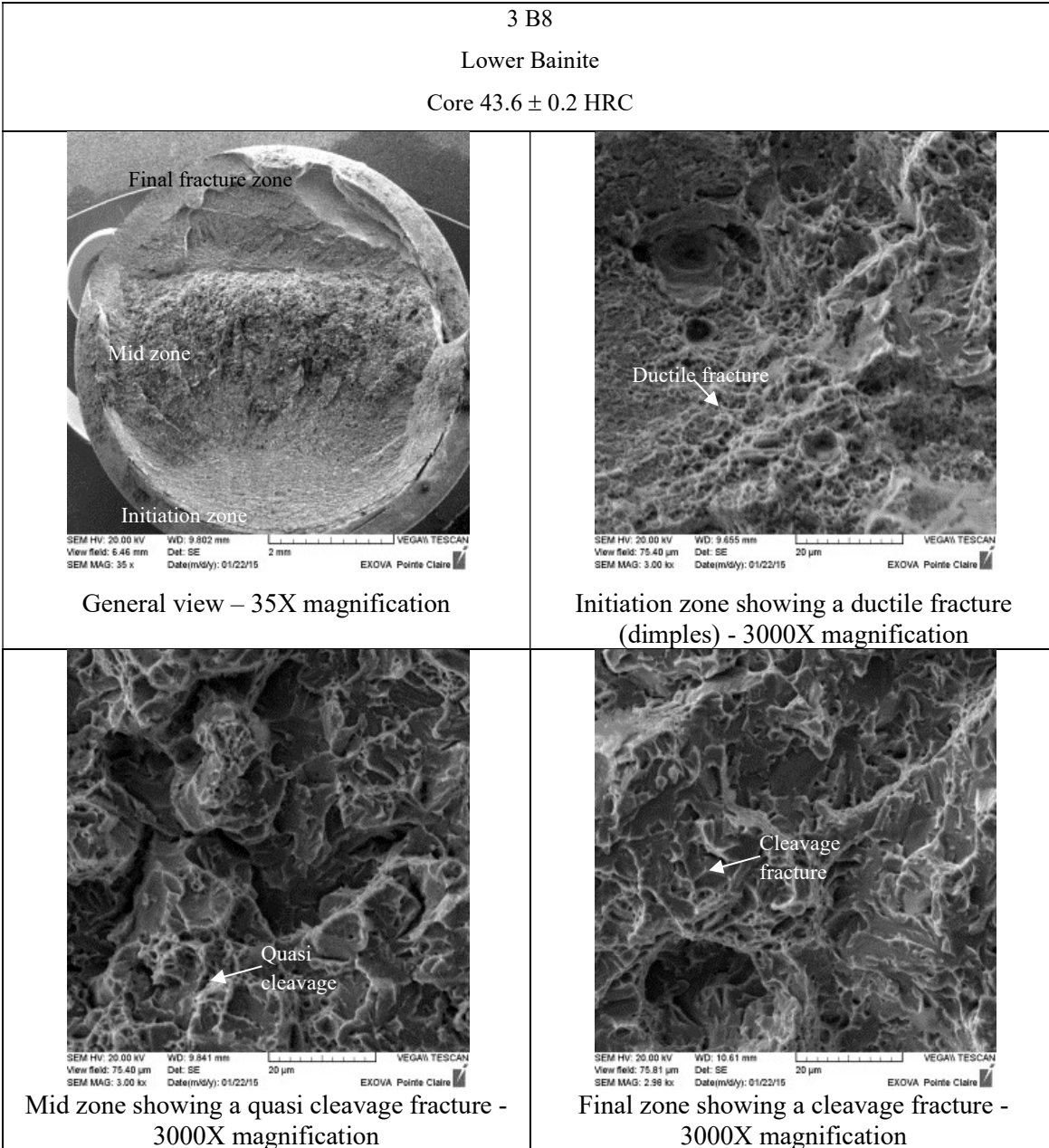


Figure A 9: Fracture surface progression during ISL evaluation of lower bainite at -1.0 V hydrogen charging condition (RAHT / High hardness).

6 B9

Tempered Martensite

Core  $43.7 \pm 0.5$  HRC

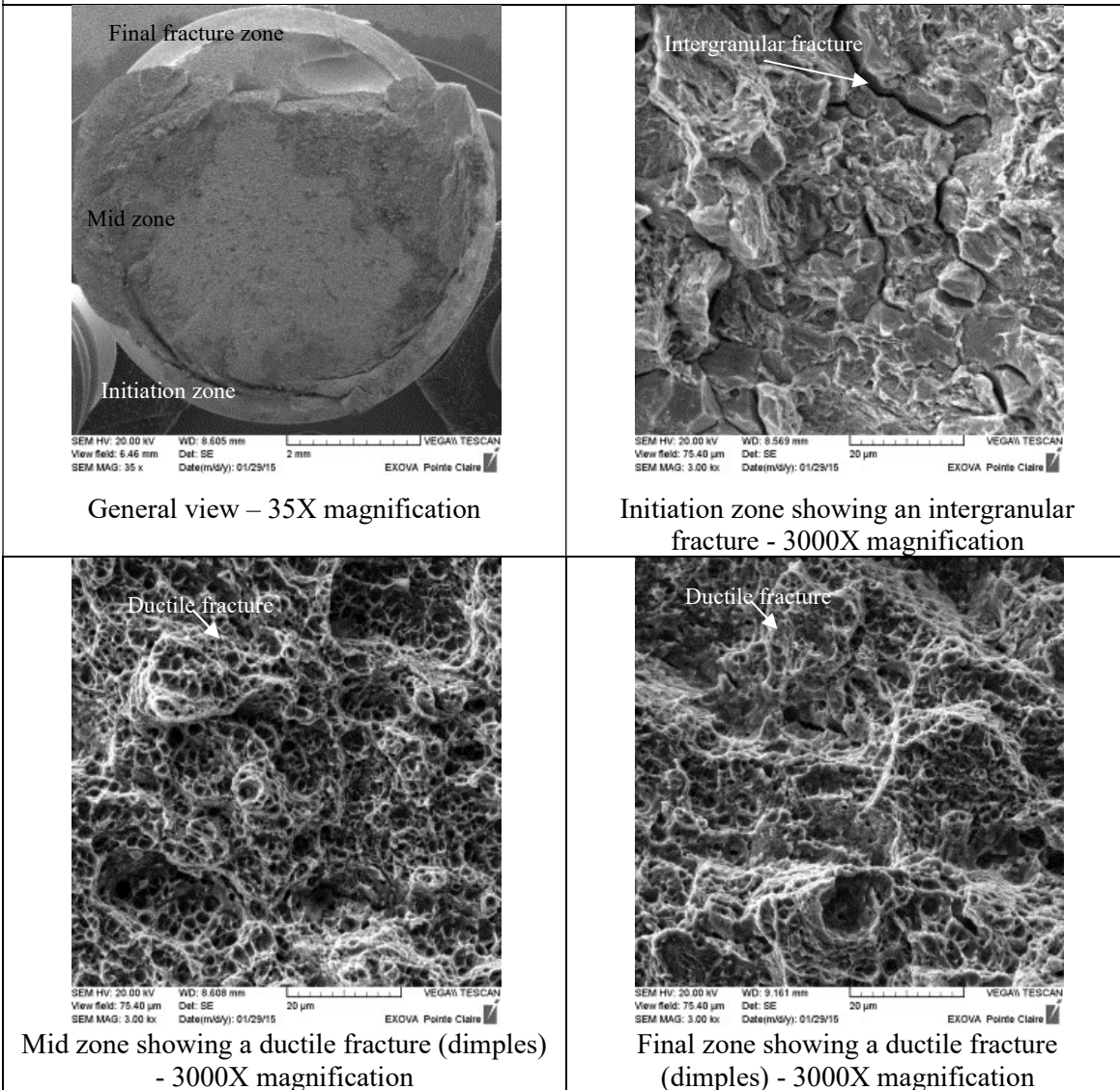


Figure A 10: Fracture surface progression during ISL evaluation of tempered martensite at -1.0 V hydrogen charging condition (RAHT / High hardness).

### A1.3 Incremental Step Loading (ISL)

Figure A 11 shows additional ISL results from tempered martensite and lower bainite samples that were RAHT at a material hardness of 39 HRC. An approximate 12% loss of fracture strength irrespective of microstructure was observed at 39 HRC at the most severe charging condition. This loss is similar to the results of approximately 11% obtained at 45 HRC (Figure 7.8) at the most severe charging condition.

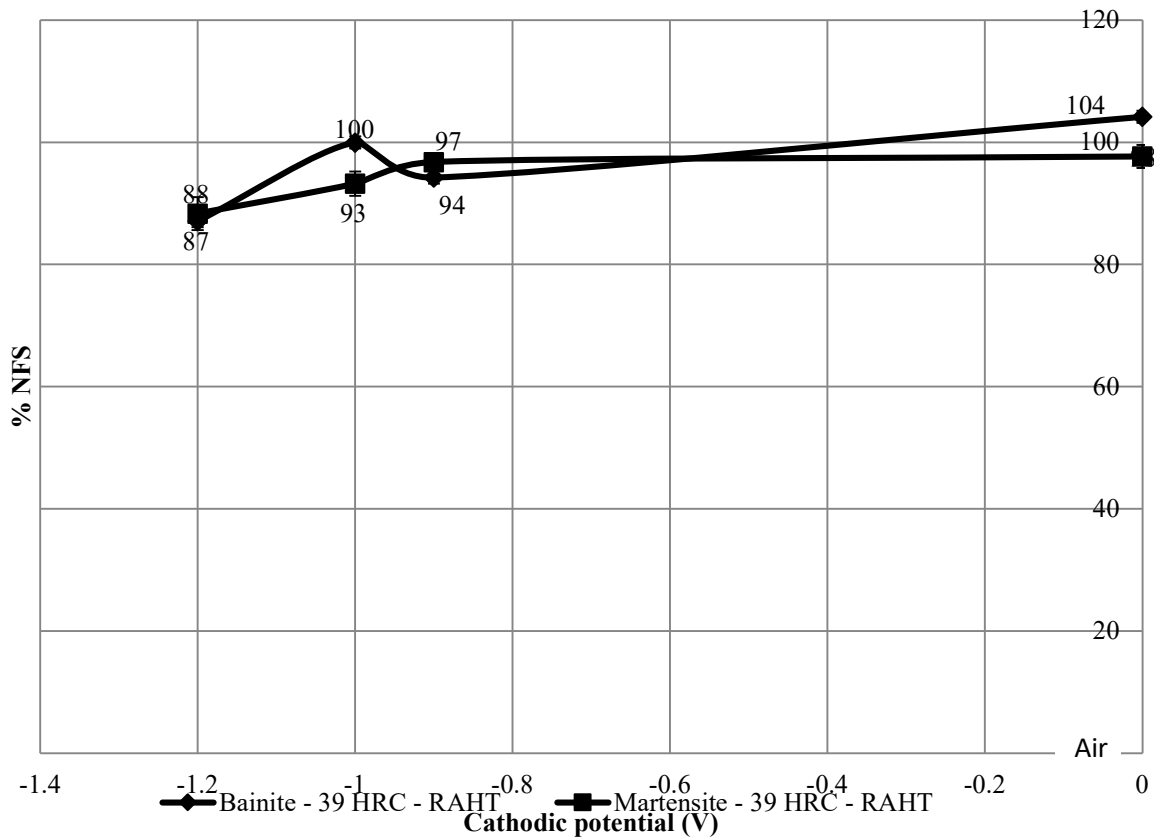


Figure A 11: NFS% drop with increasing cathodic potential for tempered martensite and bainite when rolling after heat treatment.

